Growth Technology of High-Density Carbon Nanotube Arrays for Enhanced Electric and Thermal Conduction

博士論文

Growth Technology of High-Density Carbon Nanotube Arrays for Enhanced Electric and Thermal Conduction

（電気・熱伝導促進を目指したカーボンナノチューブ高密度配列の成長技術の開発）

By Nuri Na

羅　ヌリ

A dissertation presented in fulfillment of

the requirements for the degree of

Doctor of philosophy

東京大学大学院工学系研究科化学システム工学専攻

Department of Chemical System Engineering

The University of Tokyo

August 2015

Contents

Abstract

1. Introduction

Carbon nanotubes have gathered great interests because of their various potential applications including nanoscale electronic devices due to the attractive properties of individual CNTs such as high electric and thermal conductivity, high tensile strength with flexibility, and thermal and chemical stabilities. Especially, vertically-aligned CNT (VA-CNT) arrays, grown by chemical vapor deposition (CVD) on catalyst-supported substrates, are attractive for electric and thermal transport due to their anisotropic, uni-directional structure, however they usually contain CNTs at a few vol% with air at >90 vol% [1]. To pull out the potential of CNTs, dense CNT arrays must be grown on device substrates, which changes with target applications. This research aims at development of growth technology of high-density CNT arrays on device substrates for possible applications to via interconnects in large-scale integrated circuits (LSIs) and thermal interface materials (TIMs).

2. Sub-micrometer-tall, high-density CNT arrays on conductive underlayer at 400 ℃ for LSIs [2]

CNTs are attractive as a wiring material in LSIs because they can carry electric current at a density three-orders of magnitude higher than Cu. VA-CNT arrays can be grown by CVD under various conditions, however mostly on insulating substrates at low densities of 0.03−0.07 g cm^{-3} at high temperatures of 600−800 °C [1]. To be applied to LSIs, CNTs must be grown on conductive underlayer at high density of ~ 1 g cm^{-3} at low temperature of ≤400 °C. Recently, some groups realized dense multi-wall CNT (MWCNT) arrays on conductive underlayer at

~450 °C [4,5]. However, the direct counting of the number of CNTs and their walls has not been realized yet. It is highly demanded to establish both growth and analytical methods of VA-CNT arrays.

There are two main approaches for catalyst preparation. One is to pre-form the catalyst particles and then deposit the particles on the substrate. When we attempt to deposit the catalyst densely, catalyst particles inherently deposit on the catalyst particles and/or aggregate (Fig. 1a). The other approach is to pre-form the catalyst layer on substrates and then transform the layer into particles. However, spaces inherently form between the catalyst particles (Fig. 1b). Here we propose the third approach, direct nucleation and growth of catalyst particles on substrates (Fig. 1c). When catalyst is sputter-deposited on heated substrates, catalyst adatoms diffuse over the surface, attach to each other, and nucleate particles (islands). As deposition proceeds, nucleated particles grow larger and get percolated. If deposition is stopped prior to percolation, catalyst particles can be acquired that are densely packed with minimal space between them. Even at ambient temperature, metal particles nucleate and grow during sputtering on substrates, but their density is too high to retain the high density upon heating. Preparing catalyst particles at high, but not too high, density should be key.

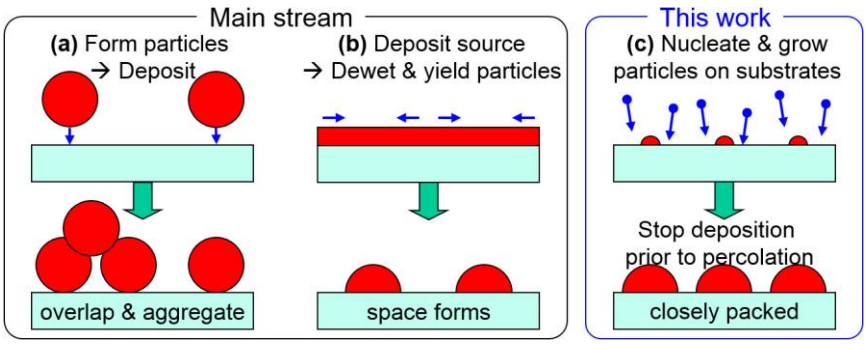

Fig. 1 Existing approaches and our strategy for preparation of catalyst particle arrays.

Based on this concept, we prepared catalyst and CNT arrays and characterized their structures in detail. Ni islands were prepared at a moderate density as deposited by enhancing the surface diffusion of Ni over TiN during sputtering at low deposition rate (8.1 pm s^{-1}), with substrate heating (400 °C) and bias voltage (−20 V), resulting in a dense Ni particle array (2.8×10^{12} cm^{-2}) after annealing at 400 ℃ (Fig. 2f). By lowering C_2H_2 pressure to 0.13–1.3 Pa so as not to kill the catalyst, dense VA-CNT arrays (~1 g cm^{-3}) were grown at a low temperature of 400 °C on the conductive TiN underlayer (Fig. 2a). Such arrays were transferred

to transmission electron microscope (TEM) microgrids or Si substrates with their roots up. Bottom-view SEM images show the densely packed CNT bundles (Fig. 2b). AFM images enabled direct counting of the roots of individual CNTs (Fig. 2c–e). HRTEM images realized direct counting of the walls within individual CNTs to be ~8. These analyses evidence that Ni catalyst particles at 2.8×10^{12} cm^{-2} grew CNTs at 1.5×10^{12} CNTs cm^{-2} and 1.2×10^{13} walls cm^{-2}. Such CNTs, formed on a conductive TiN layer at process temperatures ≤ 400 ℃ using conventional sputtering and CVD apparatuses meet many of requirements for application to via interconnects in LSIs.

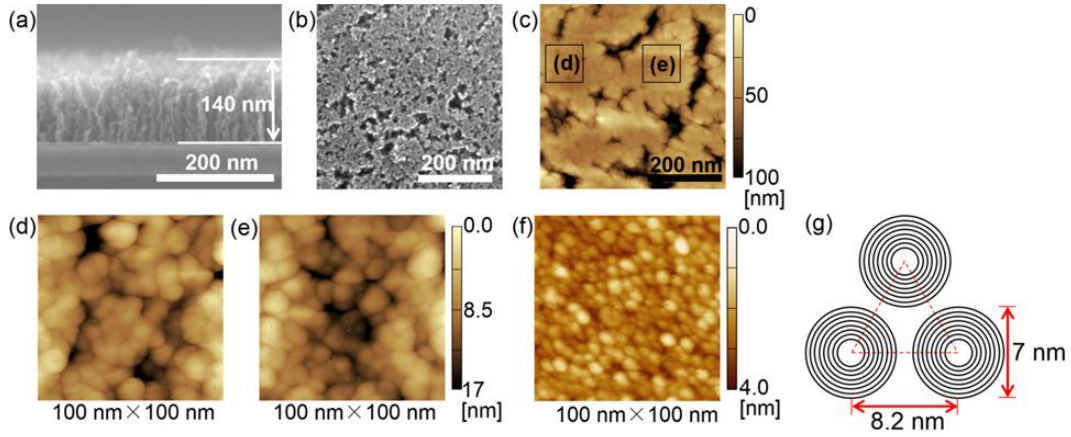

Fig. 2 Structural analyses of the dense VA-CNT arrays (~1 g cm^{-3}, 1.5×10^{12} CNTs cm^{-2}, 1.2×10^{13} walls cm^{-2}) grown at low temperature (400 °C) on conductive TiN underlayer.

3. Tens-micrometer-tall, high-density CNT arrays on both sides of Cu foils for TIMs

CNTs have high thermal conductivity and mechanical flexibility and thus their arrays on both faces of metal foils (typically Cu) are attractive as TIMs, which fill the micrometer-scale gaps between the heat sources (devices) and heat sinks. CNT arrays can be either grown directly on the foils or transferred to the foils. Such structure has been demonstrated [6], however further improvement is needed to achieve higher thermal conductivities both in the interior of the arrays and at the interface between the arrays and substrates. Fabrication of such CNT/Cu/CNT TIMs were examined by the direct CNT growth in this chapter.

To prevent the alloying of catalyst metals (Ni, Co, Fe) with Cu foils, Ta layer (being used as diffusion barrier for Cu in LSIs) and TiN layer (known effective as catalyst underlayer for

CNTs) are applied. The surface elemental composition of catalyst-supported Cu foils before and after annealing was examined by X-ray photoelectron spectroscopy. Without Ta layer, a strong Cu peak was observed with a weakened Fe peak after annealing, showing the essential role of Ta preventing intermixing of Fe and Cu. Without TiN layer, Ta peaks get evident after annealing, showing the essential role of TiN in preventing the surface segregation of Ta. This TiN/Ta bilayer with proper thicknesses (15 nm/10 nm) is essential to keep Fe catalyst particles active during CVD at 700 °C.

By optimizing the catalyst metals and thickness (Fe and 1.0−2.5 nm), and CVD temperature and C_2H_2 pressure (700 °C and 27 Pa), several-tens-micrometer-tall VA-CNT arrays were directly grown on both faces of Cu foils (Fig. 3a). The tradeoff between the height and the density of the CNT arrays are evident (Fig. 3b). As the CNT grew tall from a few to 140 μm, the mass density decreased from 0.35 to 0.1 g cm^{-3}. Relatively high density CNT arrays (0.21 g cm^{-3} at 61 μm) were realized with 2-nm-thick Fe catalyst. Then, the same approach as previous chapter, i.e. careful control of surface diffusion of catalyst during sputtering, was applied and high number density of Fe particles (8.0×10^{11} cm^{-2}) and mass density of CNT arrays (0.3 g cm^{-3} with 45 μm) were realized. The areal thermal conductivities of these CNT/Cu/CNT TIMs were evaluated (Fig. 3c). The CNT arrays enhanced the thermal conductivity from 1.5 to 4.2 W cm^{-2} K^{-1} with increasing CNT densities from 0.07–0.08 to 0.19–0.26 g cm^{-3}. This value is much better than the grease-based TIMs.

4. Conclusions

Toward practical use of VA-CNT arrays in devices, VA-CNT arrays must be formed at fairly high densities on device substrates under acceptable process temperatures. In this work, direct nucleation and growth of catalyst particles are proposed and developed, in which catalyst deposition was stopped prior to percolation, and dense catalyst particle arrays were realized even after thermal annealing. Low temperature growth (down to 400 °C) of VA-CNT arrays was achieved by moderating the C_2H_2 feed so as not to kill the catalysts. The VA-CNT arrays of high densities (1 g cm^{-3}, 1.5 CNTs cm^{-2}, 1.2×10^{13} walls cm^{-2}) directly grown on conductive TiN layer with a maximum process temperature of 400 °C meet the requirements for use as via interconnects in LSIs. The 40−60-μm-tall VA-CNT arrays of moderate densities (0.19−0.26 g

cm^{-3}) directly grown on both faces of Cu foils show enhanced thermal conductivity, which are attractive for TIM applications. Such VA-CNT arrays were realized by using conventional sputtering and CVD apparatuses. Logical design and engineering of processes meeting application requirements will put CNTs toward their practical use in society.

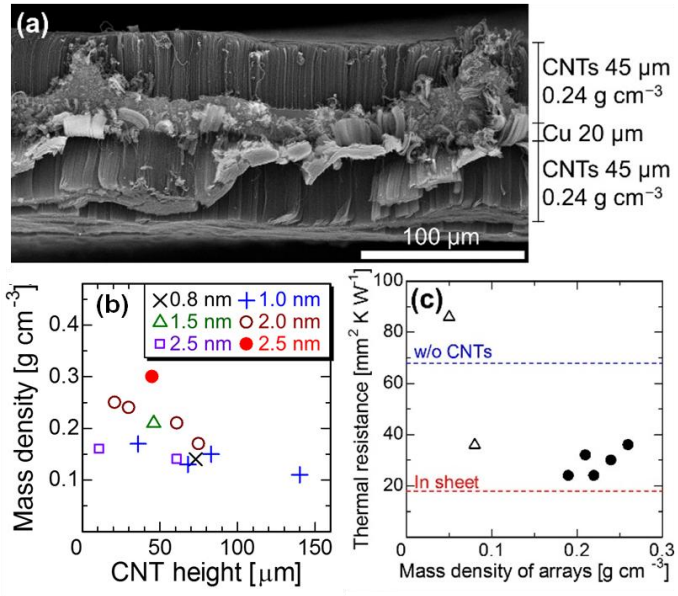

Fig. 3 CNT/Cu/CNT TIMs by direct CNT growth on Cu foils. (a) SEM image of a typical TIM. (b) CNT height vs. mass density of the CNT arrays grown at 26.7 Pa C_2H_2 and 700 ºC using Fe catalysts with various thicknesses (0.8–2.5 nm) on TiN (15 nm)/Ta(10 nm)/Cu foils (20 μm). Fe was deposited at R.T., 0 V bias, and 63 pm s^{-1} except for the sample marked with a closed red circle (2.5 nm Fe catalyst, deposited at 400 ºC, bias −20 V, and 22 pm s^{-1}). (c) Thermal resistance vs. mass density of CNT arrays.

References

[1] G. Zhong, et al., *Jpn. J. Appl. Phys.* 44, 1558 (2005).

[2] N. Na, et al., *Carbon* 81, 773 (2014).

[3] M. Nihei, et al., *Jpn. J. Appl. Phys.* 43, 1856 (2004).

[4] Y. Yamazaki, et al., *Appl. Phys. Exp.* 3, 055002 (2010).

[5] H. Sugime, et al. *Appl. Phys. Lett.* 103, 073116 (2013).

[6] B. A. Cola, et al., *Appl. Phys. Lett.* 90, 093513 (2007).

[7] N. Na, et al., *Jpn. J. Appl. Phys.* (2015), in press.

Chapter 1 - Introduction

1.1 General introduction of carbon nanotubes (CNTs)

Carbon nanotube (CNT), one of the carbon nanomaterials (fullerene, graphene), is consisted of one or multiple hollow cylinders of rolled graphene sheets. CNTs have been studied by many researchers in various area such as biotechnology, energy technology, and electronics since the Iijima's report in 1991 [1] because of their unique one-dimensional nanostructure as well as

their outstanding electrical, thermal, mechanical properties. CNTs are categorized by their number of walls composing individual CNTs, i.e. single-wall carbon nanotubes (SWCNTs) and multi-wall carbon nanotubes (MWCNTs). Generally, SWCNTs have better electric/electronic properties and are more difficult to be synthesized than MWCNTs, so the price of SWCNTs is much more expensive than MWCNTs. While all MWCNTs have metallic properties, SWCNTs have either semiconducting or metallic properties depending on their chiral index. And CNTs spontaneously form bundles each other by strong van der Waals interaction.

The resonance Raman scattering spectroscopy is one of the most popular methods for characterization of SWCNTs [2]. Two characteristic peaks appear for CNTs at around 1590 cm^{-1}, called G (graphite)-band peak, and around 1350 cm^{-1}, called D (defect)-band, and the intensity ratio of G-band to D-band peaks generally presents the crystallinity/quality of CNTs. For SWCNTs, characteristic peaks appear at the low frequency regions <400 cm^{-1}, called radial breathing mode (RBM), associated with vibrations of carbon atom in a radial direction from the CNTs. Using RBM peak, diameter (d) of SWCNT could be approximately calculated from the wavenumber (ω) by the equation, $d = 248/\omega$ [3], and the Kataura plot [4] enables us to distinguish the metallic and semiconducting SWCNTs based on the wavenumber of their peaks and the wavelength for excitation. On the other hand, in case of MWCNTs, the Raman scattering spectroscopy give us limited information; G/D ratio is sometimes used to judge their crystallinity/quality.

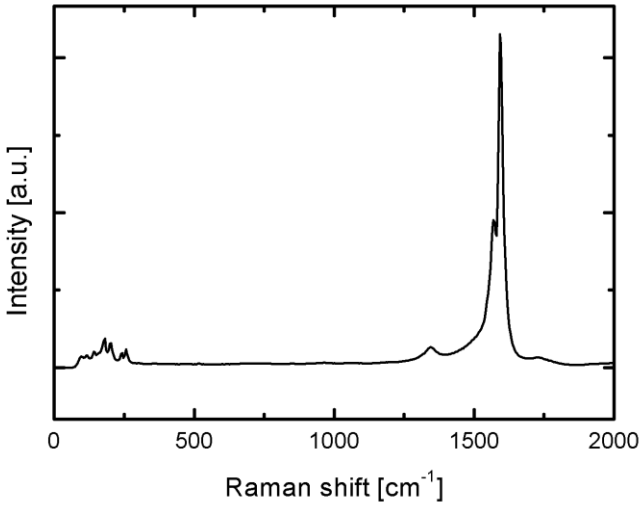

Fig. 1.1 Typical Raman spectrum of SWCNTs grown by chemical vapor deposition method.

1.2 Synthetic methods of CNTs

1.2.1 Physical vapor deposition (PVD) and chemical vapor deposition (CVD)

For over 20 years, many synthetic methods of CNTs have been reported. These methods are categorized into PVD and CVD methods based on the absence/existence of chemical reactions. In PVD methods, CNTs are formed through physical phase change; solid carbon source (typically graphite) typically with metal catalyst is heated to yield carbon and catalyst vapors at high temperatures of several thousand °C such by laser irradiation [5] or arc discharge [6, 7], and then the vapors are cooled down to yield solid carbon containing CNTs and soot. High growth temperatures allow the formation of CNTs with high crystallinity/quality. But the difficulty in scale-up due to the high process temperature and solid source materials as well as

the by-products (e.g. amorphous carbon, carbon nanoparticles) are barriers for large-scale, low-cost production of CNTs.

On the other hand, CVD methods are more widely used and considered to be more practical nowadays [8]. In CVD, carbon containing gases are fed to the reactor at moderate temperatures (600–1200 ℃, typically), decomposed normally using metal catalyst to yield CNTs. The process temperature is much lower than PVD, gaseous feedstocks can be used, and the selective catalytic reaction is possible for CNTs with little formation of by-products although the resulting CNTs sometimes have inferior crystallinity/quality than PVD. Hydrocarbons (CH_4 [9, 10], C_2H_2 [11-13], C_2H_4 [14, 15], etc.) and alcohols (mostly C_2H_5OH [16, 17]) are often used as carbon feedstock. With commonly used thermal CVD, plasma-enhanced (PE-CVD) [18], hot-filament (HF-CVD) [19] are also widely utilized for CNT growth to improve hydrocarbon decomposition. Fe, Co, and Ni are often used as catalyst for CVD due to high solubility of carbon at high temperatures and high carbon diffusion rate in these catalysts. Cu, Au, Ag Pt, Pd were also reported to catalyze various carbon feedstock for CNT growth [20].

Catalyst particles play key roles in growing CNTs; promoting the decomposition of carbon precursors at a moderate temperature and selectively yielding CNTs rather than carbon by-products (such as soot and amorphous carbon). Moreover, catalyst nanoparticles work as template for CNTs and thus enable the diameter control of CNTs to some extent although deviation is often found in the diameters of catalyst nanoparticles and CNTs [21]. Vapor-liquid-solid (VLS) mechanism is the famous model for CNT growth [22], and involves three process. First, carbon precursors adsorb and decompose on the surface of catalyst particles. Second, carbon diffuses through the bulk of catalyst particles. Finally, carbon precipitates out from the catalyst particles as CNTs. The recent in situ studies using environmental transmission electron

microscopes (e-TEM) and X-ray photoelectron spectroscopy (XPS) reveal that the catalyst can work in solid state, too, especially at low temperatures. CNT growth can also proceed through the surface diffusion of carbon over the solid catalyst nanoparticles [23, 24]. The way having catalyst nanoparticles within reactors is a key issue for enhancing productivity and controlling structures of CNTs, which is discussed in the following subsections.

1.2.2 Gas-phase synthesis by floating catalysts and on-substrate synthesis by supported catalysts

One approach having catalyst nanoparticles in the reactor is floating them in the gas flow and growing CNTs from the catalysts in the gas-phase. Such method is called floating catalyst method [25]. Ferrocene, $Fe(C_5H_5)_2$, is a popular catalyst precursor for floating Fe nanoparticle catalysts. Ferrocene vapor is fed to a furnace by a carrier gas such as H_2, Ar, and N_2, and decomposed to yield catalyst nanoparticles. During passing through the furnace, Fe nanoparticles catalyze the growth of CNTs, which are captured by filter or collected as aggregates, resulting in randomly-aligned CNT films or aggregates. Some researchers pull out CNTs mechanically from the furnace to form yarns [26]. Floating catalyst CVD enables rather high process temperatures around 1000−1400 ℃ due to the absence of reactions between catalysts and supports, and the stable CH_4 is often used as a feedstock for such high temperature not to yield soot but to yield highly-crystalline CNTs. Continuous process is possible simply by feeding the catalyst and carbon sources continuously, and mass production at ~100 ton/year per plant has been established for large diameter MWCNTs (around 100 nm or larger in diameter). Such MWCNTs are suitable for bulk use such as conductive fillers in composites and battery/capacitor electrodes. For the small diameter CNTs such as SWCNTs, however, mass

production has not been realized yet, due to the much smaller weight of SWCNTs (one SWCNT of 1 nm in diameter is four-order-lighter than MWCNT of 100 nm in diameter and the same length). Such SWCNTs show good performance when used in thin film applications such as transparent electrodes and thin film transistors in a form of random network. However, floating catalyst CVD yields CNTs inherently at random position with random orientation, and therefore it is uneasy to implement CNTs in devices with controlled positions and directions.

Another approach having catalyst nanoparticles in the reactor is supporting them on solid surfaces such as on ceramic powders (for mass production such by fluidized bed CVD [8]) and flat substrates. Especially, when we consider the application of electronic devices, direct CNT growth on device substrates are attractive. Metallic catalyst (typically Fe, Co, or Ni) is often deposited on metal oxide underlayers (Al_2O_3, MgO, SiO_2) in order to avoid the deactivation of the catalyst in the reaction with the underlayers. Various methods have been developed for catalyst preparation as introduced in Chapter 2 because preparation of catalyst nanoparticles at proper size and density is a crucial key to control the diameter and density of growing CNTs. Moreover, the resulting morphology of CNTs largely changes with the growth density of CNTs; from individuals, random networks, spikes, to forests [27]. Such structures are attractive for different applications; random networks for thin film transistors and transparent electrodes [28], spikes for field emitters [29], and forests for interconnects in large-scale integrated circuits (LSIs) and thermal interface materials (TIMs) [30, 31]. Among them, this work targets at the forests, which are discussed in the next sub-section 1.2.3.

1.2.3 Vertically-aligned CNT arrays on substrates by CVD

Vertically-aligned CNT (VA-CNT) arrays on substrates have efficient morphologies for transport of electricity or heat owing to their oriented nature. They were realized first for MWCNTs using Fe catalyst supported on mesoporous silica; MWCNTs of 30 nm in diameter, 50 μm in length by CVD for 2 h in 1996 [32] and those of 30 nm in diameter, 2 mm in length by CVD for 48 h in 1998 [33]. Several years later, such growth was realized for SWCNTs; several-μm-tall VA-SWCNTs were realized by Co-Mo catalyst dip-coated on quartz glass substrate by alcohol catalytic CVD using C_2H_5OH feedstock in 2002 [17], and millimeter-tall VA-SWCNTs were realized by Fe/Al_2O_3 catalyst sputter-deposited on SiO_2/Si by water-assisted CVD (so-called Super Growth) using C_2H_4 feedstock in 2004 [14].

Normally, CNT arrays on substrates grown by CVD have very porous structures (>90 vol%), and thus growth of high-density arrays is necessary for many of their applications. Therefore, in order to obtain high-density CNT arrays on substrates, we have to not only form dense catalyst particles, but maintain activity of the catalyst particles during CVD. The density variation of VA-CNT arrays with growth time was demonstrated [34, 35]. The VA-CNT densities increase during nucleation of CNTs, keep constant during steady growth, and finally decay at growth termination [35]. There are various reasons of growth termination, such as ripening or coarsening, and I will discuss these in Chapters 2 and 3.

1.3 Application targets of CNT arrays of this work

The targets of this research are via interconnects in LSIs and TIMs. While CNT arrays have preferable properties and morphologies for these applications, several issues have to be solved.

1.3.1 Via interconnects in large-scale integrated circuits (LSIs)

Currently, Cu is utilized for wiring in LSIs. However, scaling down of the dimensions of LSIs caused difficult issues; increasing resistivity in Cu wiring due to the increasing surface to volume ratio and electro-migration due to the increasing current density. On the other hand, CNTs have received attention as alternative materials for interconnects since they can carry current at high density (10^9 A cm^{-2}, 100–1000 times higher than Cu) without scattering at the sidewalls.

Nevertheless, CNTs presently do not have sufficiently low electrical resistance to replace Cu. The main reason is that the number of conduction channels (the number of walls in CNT bundles) is insufficient, so growth of high-density CNT arrays is a critical issue. Furthermore, CNTs must be grown at 400 ℃, much lower than typical CNT growth temperature of 700−850 ℃, to be compatible with LSI process.

1.3.2 Thermal interface materials (TIMs)

Since power density of electronic devices continually increases, thermal management is also becoming a critical issue in order to improve the performance while keeping the reliability of devices. Thermal interface materials (TIMs) play a key role in transferring the heat from the

small ULSI chips to the big heat sinks by enhancing thermal conduction between the two solid surfaces. Currently, grease based TIMs are used commercially, which realize excellent areal contacts due to their fluidity but small thermal conductivity (0.7–3 W m^{-1} K^{-1}) due to the matrix grease. Also, "pump-out" occurring during power cycling, induces degradation of TIMs.

On the other hand, CNTs are a candidate for future TIMs owing to their high thermal conductivities (3000–6000 W m^{-1} K^{-1}) [36, 37], very stable in changing temperature during power on and power down, and mechanical flexibility. Especially, CNT array TIMs have received great attention because their configuration structures have advantages of high mechanical compliance and high thermal conductivity (10–200 W m^{-1} K^{-1}) [38-40]. However, for further low thermal resistance, increasing number density of CNTs is a quite important issue same as CNT via interconnects. And growth technologies of CNTs on metallic substrates or foils have to be established.

1.4 Objectives

When CNT arrays are directly grown on devices, CNT structures and growth conditions should meet all of the requirements from the devices. And this research deals with two applications; via interconnect in LSI and TIM.

First of all, growth of high-density CNTs is demanded in both applications because air is electrically and thermally insulating.

Second, a length of CNT arrays is also a crucial factor. Sub-μm-length is enough for via interconnect application, but several tens of μm would be necessary in case of CNT array TIMs according to roughness of joining surfaces.

Third, in via interconnect application, acceptable growth temperature is limited as low as 400 ℃ in order to avoid any damage to LSIs. In TIM application, however, this limitation could be avoided because CNT arrays are grown on difference substrates from devices.

Forth, underlayer also should meet some requirements. In via inter connect application, CNT arrays have to be grown on conductive underlayers instead of metallic oxide underlayers to be used as wiring in electronic devices. On the other hand, in TIM application, growing of CNT arrays on metallic foils is needed.

Therefore, we have developed technologies of catalyst deposition and CVD to meet these requirements.

Chapter 2 - Sub-Micrometer-Tall, High-Density CNT Arrays on Conductive Underlayer at 400 °C for LSIs

2.1 Introduction

VA-CNT arrays [14, 15, 41, 42] have gathered interest because of their potential application in nanoscale electronic devices [43, 44]. In particular, via interconnects in LSIs using densely packed CNT arrays are attractive because CNTs can carry electric current at a high current density (~10^9 A cm^{-2}) [45] without scattering at the sidewalls of the interconnects [46]. This cannot be achieved by currently available Cu interconnects. CNTs also possess an excellent conduction channel for each wall and, therefore, putting CNT walls as much as possible in the via holes becomes a key issue for realizing interconnects with low resistivity and high current-carrying capacity.

For perfect, closely packed, SWCNT arrays, a high number density of ~1×10^{14} cm^{-2} is expected. However, SWCNTs normally contain a larger fraction of semiconducting tubes than metallic tubes (semiconducting tubes : metallic tubes 2:1 for SWCNTs of random chirality) [47, 48], making the situation unsuitable for electrical conduction. Furthermore, it is technologically difficult to realize 1-nm-sized catalyst particles at a number density of ~1×10^{14} cm^{-2} because particles must have a spacing much smaller than 1 nm and such small particles easily aggregate. Indeed, millimeter-tall dense SWCNT arrays are commonly very porous (porosity >0.9) with an areal density of ~1×10^{12} cm^{-2} and a mass density of 0.03—0.07 g cm^{-3} [42, 49]. However, multi-wall CNTs (MWCNTs) always exhibit metallic properties as a result of the interaction between neighboring walls [50]. For example, an array of MWCNTs with a 4-nm diameter, 5 walls, and 4×10^{12} cm^{-2} areal density has a high wall density of 2×10^{13} cm^{-2} while an array of catalyst particles with a diameter of 4 nm and areal density of 4×10^{12} cm^{-2} can have a spacing ≥1 nm. Thus, such structures, i.e., dense arrays of MWCNTs, are good candidates for interconnects.

Production process is also important. Vertically aligned CNT arrays are often formed at high CVD temperatures of 600—800 ℃ on insulating underlayers such as Al_2O_3 [14, 15, 41, 42, 49, 51, 52]. However, CNTs should be synthesized on a conductive layer to be useful as interconnects, and at low temperatures (~400 ℃) to avoid any damage to LSIs. The three requirements, i.e., high wall density ~10^{13} cm^{-3}, low CVD temperature ≤400 °C, and being on a conductive underlayer need to be satisfied to realize the practical application of CNT-based via interconnects in LSIs.

Awano and coworkers have pioneered work into CNT interconnects [30, 53-55]. They developed a cluster deposition method [53] in which catalyst particles are formed by laser

ablation, size selected, and then introduced into the bottom of the via holes as a cluster beam. This approach can realize the growth of MWCNT arrays at a density of ~3×10^{11} cm^{-2} from the bottom of the via holes at the low temperature of 450 ℃ [54]. Later, they developed a multi-step growth method [55], whereby in the first step, a H_2 or Ar plasma is applied to a Co catalyst layer on a conductive TiN/Ta barrier layer on Cu to induce Co particle formation at 25—260 ℃. A CH_4/H_2 plasma is then applied to nucleate CNTs at 170—350 ℃, before finally a CH_4/H_2 plasma is applied to grow CNTs at 450—600 ℃. By observing the cross-section of the CNTs using a scanning electron microscope (SEM), they estimated the areal density to be as high as ~1×10^{12} cm^{-2} for the CNT arrays produced via this multi-step process at 450 ℃. Zhong, Robertson, and coworkers have also extensively researched in this area [56-58]. They used an $Al_2O_3/Fe/Al_2O_3$ sandwich catalyst [56] and grew SWCNTs, reporting on high-density SWCNT arrays [57]. By assuming the absence of carbon byproducts and the SWCNTs to be perfectly straight, they estimated, indirectly from the film weight and the SWCNT diameter, the areal density of these SWCNTs to be as high as ~1.64×10^{13} cm^{-2}. Because the SWCNT arrays were grown on an insulator at a CVD temperature as high as 700 ℃, this method does not meet the requirements for via interconnects in LSIs. Recently, Sugime et al. reported on MWCNT arrays with a mass density as high as 1.6 g cm^{-3} using the Co-Mo co-catalyst on a conductive Ti-coated Cu layer at a rather low CVD temperature of 450 ℃ [58]. This achievement is closer to the application requirements and, thus, encouraging, but the areal density of CNTs and their walls have not yet been determined. Both the growth of CNTs that meet the process and structure requirements (≤400 °C, ≥1×10^{13} walls cm^{-2}, on a conductive underlayer) and the direct determination of the areal density of CNTs and their walls remain challenges.

In this work, we propose a simple process that meets the requirements and introduce a detailed structure analysis that directly illustrates that the CNT and wall densities achieve the structure requirements.

2.2 Experimental

Si wafer with a 50-nm-thick thermal oxide (SiO_2) layer was cleaned using a 3:1 solution of sulfuric acid (H_2SO_4) (98 wt%) and aqueous hydrogen peroxide (H_2O_2) (30 wt%) and used as the substrate. A 5-nm-thick TiN conductive underlayer was deposited by radio frequency sputtering with a Ti target in N_2/Ar, and then Ni with a 0.6-nm nominal thickness was immediately deposited onto TiN by direct current sputtering with an Ni target in Ar without breaking the vacuum. A magnetron sputtering apparatus (MPS-2000HC2S; ULVAC, Chigasaki, Japan) with a base pressure $\leq 2 \times 10^{-6}$ Pa was used for both depositions. Various deposition conditions were investigated for Ni: temperatures (room temperature and 400 ℃), deposition rates (8.1 pm s^{-1} and 34 pm s^{-1}), and substrate bias (0 and −20 V). Deposition rates were controlled by changing the discharge power between 10 and 50 W for the 2-inch Ni target.

CNTs were grown by CVD using nominally 0.6-nm-thick Ni catalyst deposited on 5-nm-thick TiN at 400 ℃ and 8.1 pm s^{-1} with −20 V substrate bias. After the catalyst deposition process, substrates were set in a tubular quartz glass, CVD reactor (34-mm inner diameter, 300-mm length) [51, 59] and annealed with pure H_2 (30 sccm) at 1.3 kPa during heating to 400 ℃ and keeping at this temperature for 8 min. Finally, CVD was carried out at a rate of 180 sccm for 5–60 min by switching the gas to 0.13–1.3 Pa C_2H_2 with Ar balance gas at 0.27 kPa.

The catalysts before and after annealing were analyzed by atomic force microscopy (AFM; SPM 9600; Shimadzu, Kyoto, Japan) and the number densities of the particles were derived from the AFM images. The resulting CNTs were characterized using a field emission SEM (S-4800; Hitachi, Tokyo, Japan) equipped with an energy dispersive X-ray spectrometer (EDS; EDAX Genesis; AMETEK, Berwyn, PA, USA) and high-resolution transmission electron microscopy (HRTEM; JEM-2800; JEOL, Akishima, Japan). Some CNT films were separated from the substrate by etching the Ni/TiN/SiO_2 layer using HF (25 wt%) solution and transferred to Si substrates or TEM microgrids with their bottom up (upside down). These were analyzed by SEM and AFM to take the bottom view images and by TEM to take the transmittance images perpendicular to the film surface. The absence of Ni/TiN/SiO_2 at the roots of the transferred CNT arrays was confirmed by X-ray photo electron spectroscopy (XPS; PHI Versa Probe II; ULVAC-PHI, Chigasaki, Japan) using a monochromatized Al Kα X-ray source and a 45° detection angle. The amount of carbon (g cm^{-2}) was determined by the C to Si peak area ratios by SEM-EDS analysis at an acceleration voltage of 5 kV, and using the film thickness (cm) to determine the mass density of the CNT films (g cm^{-3}). Sputtered carbon films on Si substrates were used as a reference for the EDS analysis (Fig. 2.1), where the density was determined by X-ray reflection measurement (ATX-G; Rigaku, Akishima, Japan) to be 1.66 g cm^{-2}.

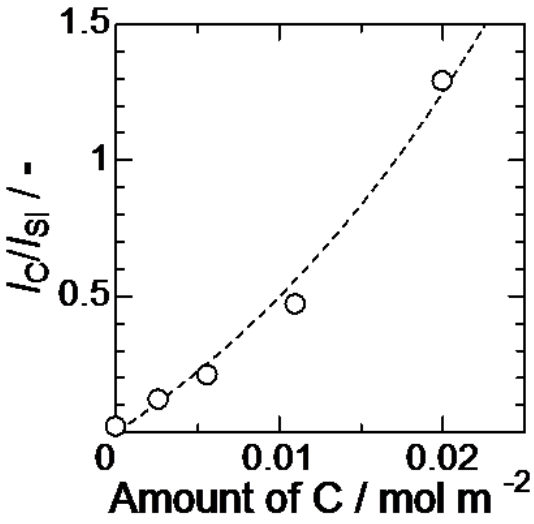

Fig. 2.1 Calibration curve for the amount of carbon detected by SEM-EDS. Amorphous carbon films sputter deposited onto the SiO_2/Si substrates, with a mass density of 1.66 g cm^{-3}, were used. The amount of carbon in the CNT arrays was determined by first determining the intensity ratio of C to Si (I_C/I_{Si}) by SEM-EDS and then converting it to the amount of carbon using this calibration curve. SEM-EDS was performed with an acceleration voltage of 5 kV for all samples.

2.3 Results and discussion

2.3.1 Preparation of dense catalyst particle arrays through nucleation and growth during sputtering

We first designed the catalyst preparation method. As shown in Fig. 2.2(a,b), there are two main approaches for catalyst preparation. One is to pre-form the catalyst particles and then deposit the particles on the substrate, such as by the cluster deposition method [53], and wet coating of the colloidal catalyst particles [60]. When we attempt to deposit the catalyst densely, catalyst particles inherently deposit on the catalyst particles and/or aggregate (Fig. 2.2(a)) unless some countermeasure, such as the use of oxide particles, is applied [60]. The second

approach is to pre-form the catalyst layer on substrates and then transform the layer into particles. Although extensive efforts have been made to form catalysts at high densities using plasma treatment [55-57], spaces inherently form between the catalyst particles (Fig. 2.2(b)). Therefore, we herein propose an alternative approach, namely direct nucleation and growth of catalyst particles on substrates (Fig. 2.2(c)). When we sputter catalyst on heated substrates, catalyst adatoms diffuse over the surface, attach to each other, and nucleate particles (islands). As deposition proceeds, nucleated particles grow larger and get percolated. If we halt deposition prior to percolation, we may obtain catalyst particles that are densely packed with minimal space between them. Even at ambient temperature, metal particles nucleate and grow during sputtering on substrates [61, 62], but their density is too high to retain the high density upon heating (Fig. 2.2(d)). Preparing catalyst particles at high, but not too high, density should be key (Fig. 2.2(e)).

When atoms of catalyst are deposited on substrates, they become adsorbed at the surface of substrates as adatoms. Adatoms travel over the surface with the diffusion coefficient, and combine with one another to form a particle. During this process, the size of particle is decided by surface diffusion length of adatoms and quantity of catalyst adatoms within surface diffusion length. If diffusion length is too short or quantity of catalyst adatoms is too much within surface diffusion length, morphology of deposited catalyst is continuous films as deposition. Continuous films are changed particles according to thermal annealing. However, in this case, the number density of particles is low because there is a gap between particles. On the other hand, if diffusion length is too long or quantity of catalyst within surface diffusion length is insufficient, particles are formed before thermal annealing, but they are too small to synthesis of

CNTs. Therefore, we form dense catalyst particles through control of surface diffusion length and amount of deposited catalyst during deposition process.

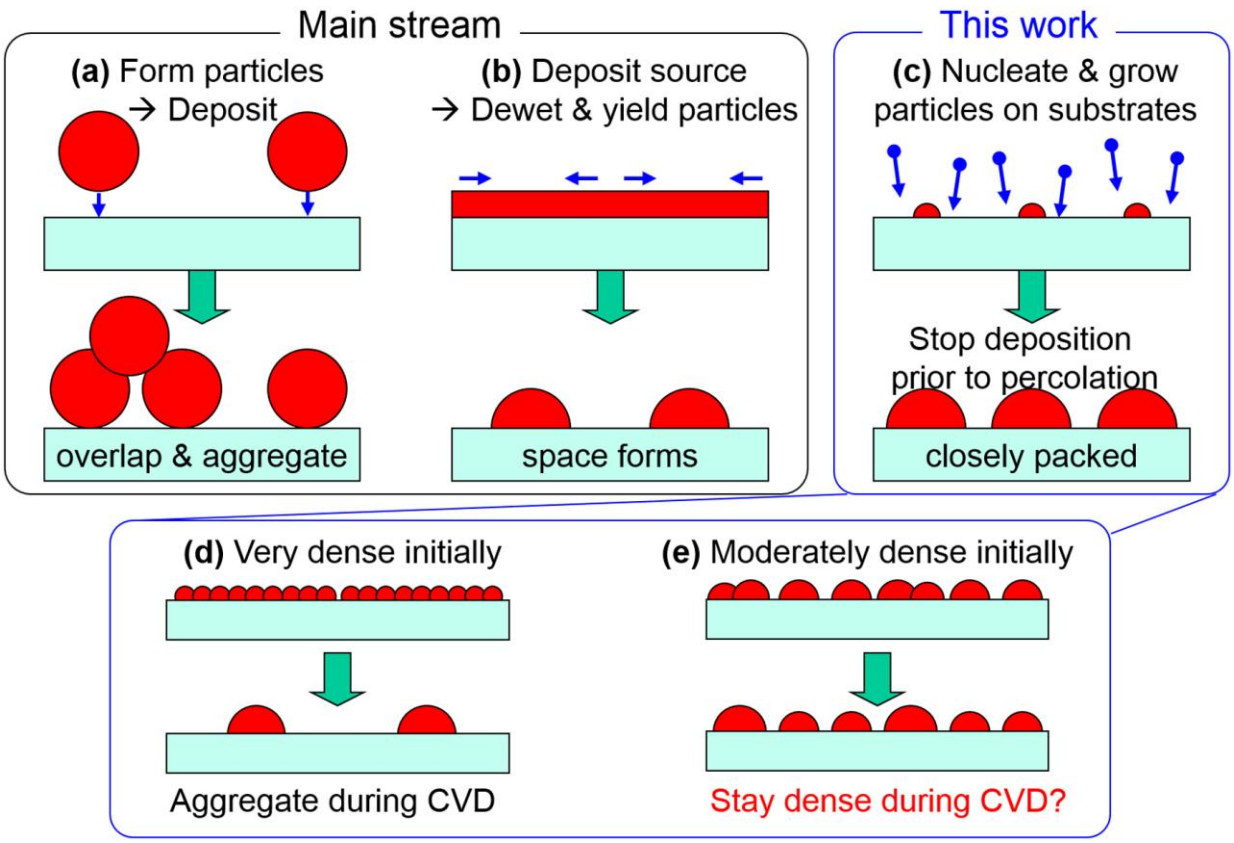

Fig. 2.2 Approaches for preparation of catalyst particle arrays on substrates. (a) Pre-forming catalyst particles and then depositing the particles on the substrate. (b) Pre-forming the catalyst layer on substrates and then transforming the layer into particles. (c) Directly nucleating and growing catalyst particles on substrates. (d,e) Our strategy for maintaining catalyst particles at high densities during CVD.

Based on this concept, we carefully examined the catalyst preparation. The requirement of low CVD temperature is beneficial for preparation of dense catalyst particles on conductive underlayers because both catalyst deactivation as a result of alloying with the underlayer and coarsening through Ostwald ripening [11, 63] can be prevented at low temperatures. We selected TiN [55], which is frequently used as a barrier material in LSIs, as the conductive underlayer and deposited Ni onto it.

Fig. 2.3(a) shows the AFM images obtained of the nominally 0.6-nm-thick Ni deposited onto 5-nm-thick TiN on SiO_2/Si substrates. Of the systems studied herein, Ni deposited at ambient pressure and at a high rate of 34 pm s^{-1} had the finest structure at deposition but had the most pronounced particulate structure with a particle number density of 1.2×10^{12} cm^{-2} after annealing under H_2/Ar at 400 °C for 10 min (Fig. 2.3). An increased deposition temperature of 400 °C, which enhances the surface diffusion of Ni, yielded a rougher structure as deposited but kept the finer particulate structure with the increased particle number density of 1.6×10^{12} cm^{-2} after annealing (Fig. 2.3(b)). A similar effect was observed for a decreased deposition rate of 8.1 pm s^{-1}, which allows Ni adatoms to diffuse for a longer period of time, yielding particles at 1.9×10^{12} cm^{-2} after annealing (Fig. 2.3(c)).

The combination of high deposition temperature (400 °C) with low deposition rate (8.1 pm s^{-1}) realized even denser particles at 2.4×10^{12} cm^{-2} (Fig. 2.3(d)). Finally, application of a substrate bias voltage of −20 V, which further enhances the surface diffusion of Ni by irradiation of cationic species [64], in addition to the high deposition temperature and low deposition rate, made particles with the highest density of 2.8×10^{12} cm^{-2} after annealing (Fig. 2.3(e)). The particle arrays having the highest (Fig. 2.3(a)) and lowest densities (Fig. 2.3(e)) as deposited, which yield particles at the lowest and highest densities, respectively, after annealing, are shown with a modified height scale in Fig. 2.3(f,g) for comparison. It should be noted that catalysts for CNT growth are often deposited at room temperature and high deposition rates, which correspond to the conditions for Fig. 2.3(a). This may be one reason why catalyst particles formed from a sputtered layer by annealing are often not particularly dense (around 1×10^{12} cm^{-2}) [12, 49]. These results support the concept that to yield dense particle arrays after

annealing (and thus prior to CVD), the initial Ni layer should be formed at a moderate island density by promoting the surface diffusion of Ni.

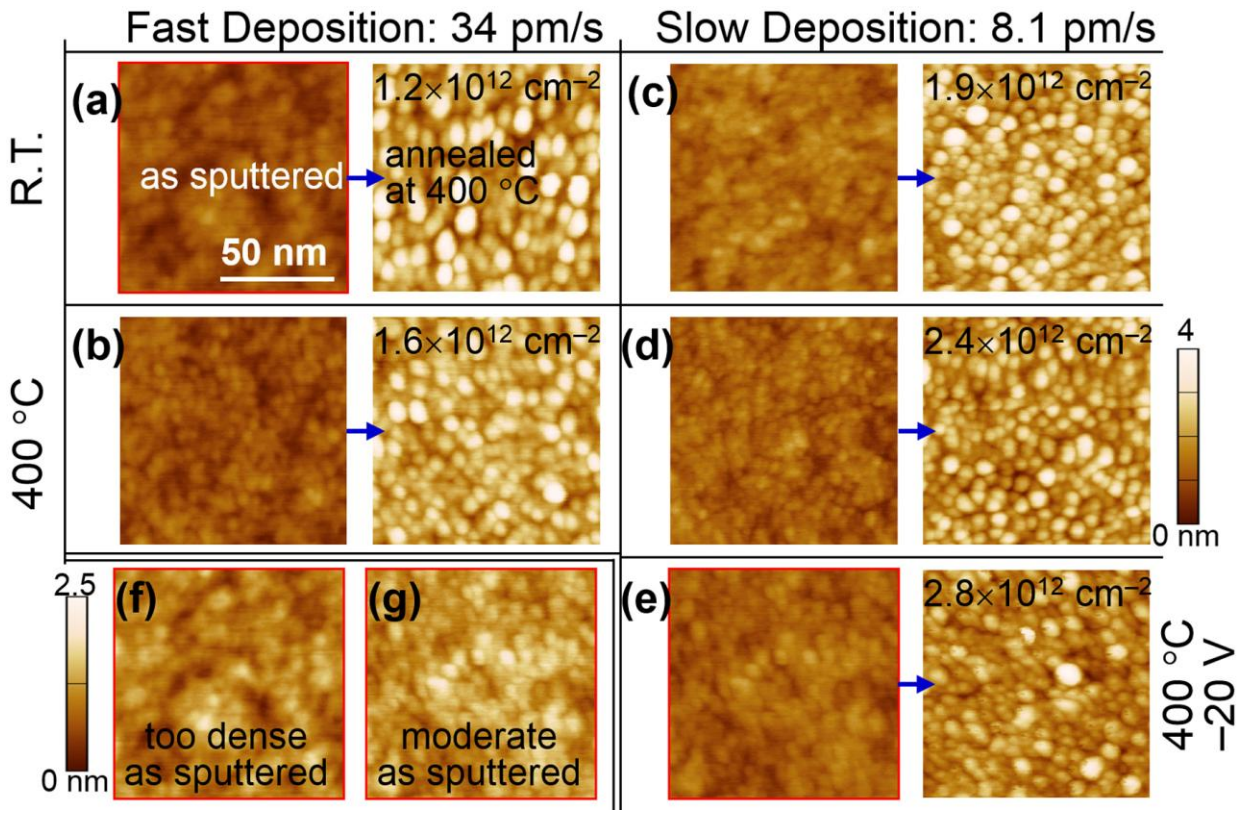

Fig. 2.3 (a-e) AFM images of Ni particles deposited at different temperatures and deposition rates. The number densities of the Ni particles are shown in the images after annealing at 400 ℃ for 10 min. (f,g) The AFM images shown at a magnified height scale. (f) and (g) are of the same images as those as deposited (as sputtered) in (a) and (e), respectively. The scale bar for the lateral dimension in (a) applies for all images. And the scale bar for the height in (d) applies for the images (a–e).

Of course, excess promotion of surface diffusion causes as-deposited islands to be too large and sparse, which is unsuitable for CNT growth. If the as-deposited catalyst shows an isolated particulate structure, surface diffusion needs be suppressed. In contrast, if the as-deposited catalyst shows a continuous film structure, surface diffusion needs to be promoted. Optimization of surface diffusion and nominal catalyst thickness are important for providing dense catalyst particle arrays. The 0.6-nm-thick Ni catalyst deposited on 5-nm-thick TiN at

400 °C and 8.1 pm s^{-1} with −20 V substrate bias was used to grow CNTs by CVD in the following sections.

2.3.2 Low temperature growth of CNT arrays by limiting C_2H_2 feed

Various carbon containing species, such as C_2H_2 [11-13], C_2H_4 [14, 15], and C_2H_5OH [16, 17], can be used as feedstock for millimeter-tall, vertically aligned CNT arrays. However, C_2H_2 directly fed or forming through the decomposition of hydrocarbon/alcohol has been proven to be an efficient direct precursor for growth of such arrays [16]. Coarsening of catalyst particles through Ostwald ripening and carbonization of catalyst particles as a result of the excess carbon feed are important deactivation mechanisms. While the former is suppressed at lower temperature, the latter gets more significant at lower temperature and, thus, the C_2H_2 should be fed at lower partial pressures for lower CVD temperatures [11]. Hence, we fed 0.13–1.3 Pa C_2H_2 at 400 °C, which is two to three orders of magnitude lower than that for the millimeter-tall CNT arrays at 800 °C in previous studies [11-13]. Fig. 2.4 shows cross-sectional SEM images of the CNT arrays grown on the conductive TiN underlayer for different growth times and C_2H_2 partial pressures. CNTs grew in vertically aligned arrays under all of the conditions examined. CNTs were shorter for the lower C_2H_2 pressures at the initial stage of 5–10 min, while they became similar in height at the later stages (30–60 min). There are some differences in the surface smoothness obtained at these different conditions: CNT arrays had a rough surface with 0.13 Pa C_2H_2 (Fig. 2.4(a–d)), whereas they had a smooth surface with 1.3 Pa C_2H_2 (Fig. 2.4(e–h)). We also examined the growth of CNT arrays using C_2H_2 at even lower pressure (0.04 Pa), and found that CNT arrays grew taller over time until 60 min, even though their alignments and

mass densities were not desirable (Fig. 2.5). These results show that CNTs nucleate more quickly and grow faster but stop growing earlier for higher pressure C_2H_2 feed.

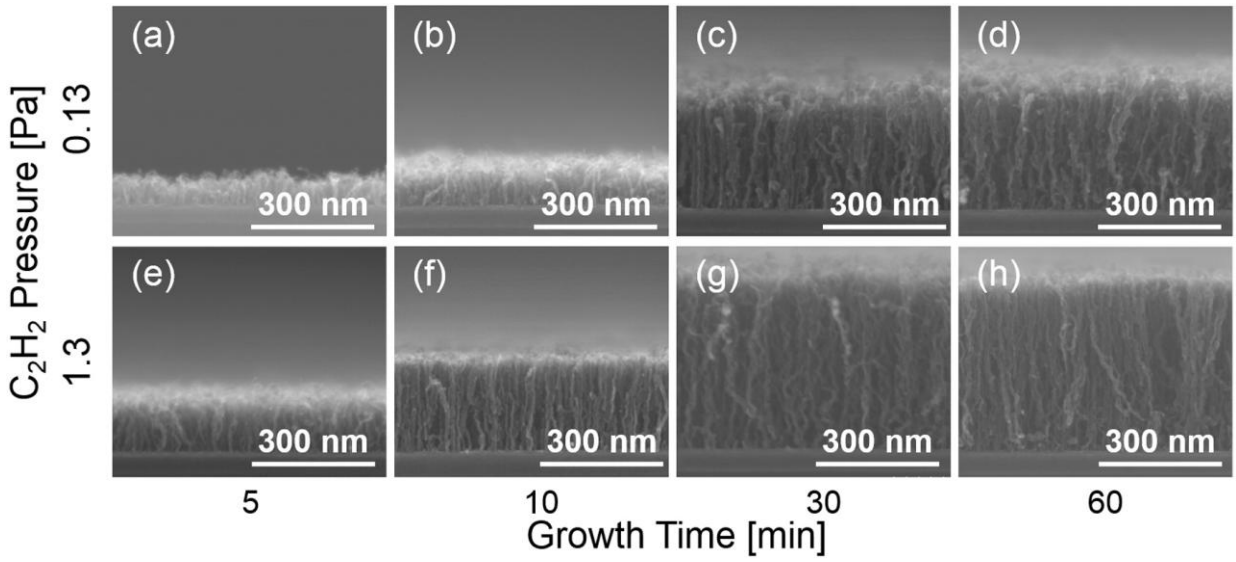

Fig. 2.4 Cross-sectional SEM images of CNTs grown by Ni catalyst on TiN at 400 ℃ from (a–d) 0.13 Pa and (e–h) 1.3 Pa C_2H_2 for (a,e) 5, (b,f) 10, (c,g) 30, and (d,h) 60 min.

Next, we carefully characterized the average height, areal density, and mass density of the CNT arrays for growth times of 5–30 min (when CNTs keep growing) (Fig. 2.6). The height of the CNT arrays continuously increased with growth time until about 30 min for both the 0.13 and 1.3 Pa C_2H_2 pressures (Fig. 2.6(a)). However, the amount of carbon almost stopped increasing after a growth time of 20 min for the higher C_2H_2 pressure (1.3 Pa) (Fig. 2.6(b)). This result suggests that the significant fraction of Ni catalyst particles were deactivated within 20 min with 1.3 Pa C_2H_2, and the CNTs are growing at a low density from 20 to 30 min at the bottom of the CNT array, lifting up the pre-formed dense array. In contrast, the amount of carbon increased over the period of 20–25 min for the lower C_2H_2 pressure (0.13 Pa) (Fig. 2.6(b)), indicating that a significant fraction of the catalyst particles remained active for 20 min or more. From the CNT height and amount of carbon, we calculated the mass density of the CNT arrays.

It was initially as high as 1.0 g cm^{-3} (5–10 min) but decreased to ~0.75 g cm^{-3} after 30 min for both 0.13 and 1.3 Pa C_2H_2 (Fig. 2.6(c)).

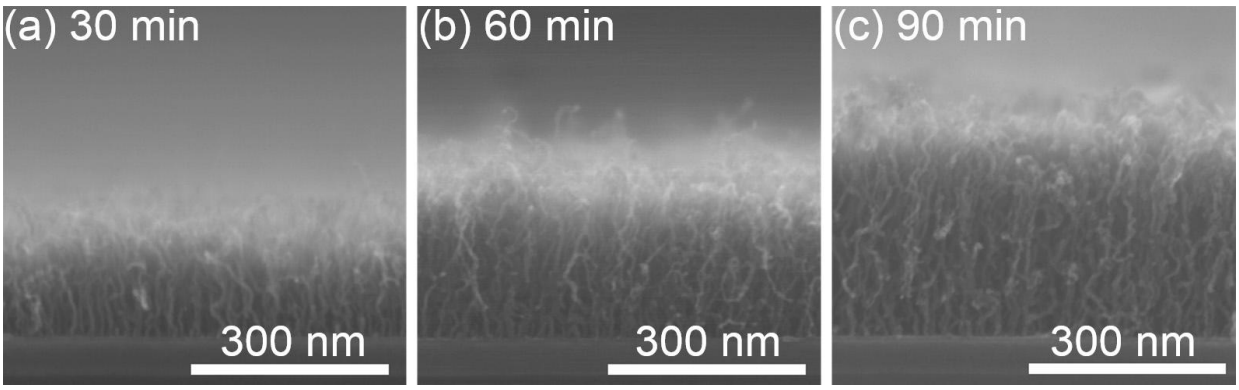

Fig. 2.5 Cross-sectional SEM images of CNT arrays grown by Ni catalyst on TiN at 400 ℃ from C_2H_2 at a very low partial pressure of 0.04 Pa for ~90 min. CNTs grew continuously for a long period but at a low density with rather poor alignment.

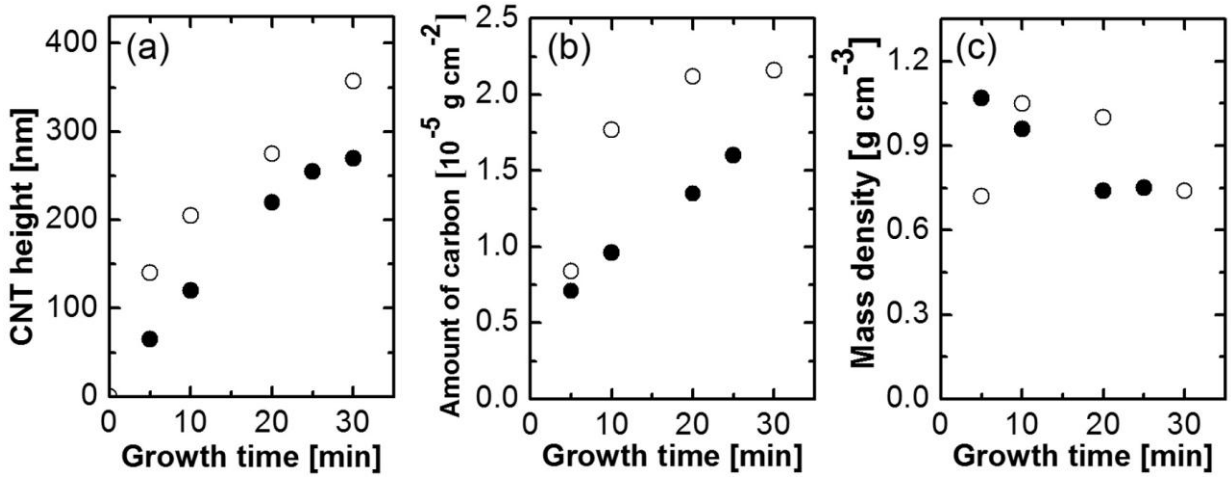

Fig. 2.6 (a) Height, (b) amount of carbon, and (c) mass density of the CNT arrays grown by Ni catalyst on TiN at 400 ℃ from 0.13 Pa (black dot) and 1.3 Pa (white dot) C_2H_2. The mass densities of the CNT arrays were initially 0.7–1.1 g cm^{-3} and decreased to ~0.75 g cm^{-3} after 30 min for both 0.13 and 1.3 Pa C_2H_2

2.3.3 Evaluation of the number densities of CNTs and CNT walls

Of key importance is the areal density of the CNT walls, which provide the electrical conduction channels; however, this has not yet been directly evaluated. CNT arrays commonly have a disordered part at their top and, thus, it is difficult to count the number of CNTs within the array. Here, we realized the direct observation of the CNT roots and CNT walls within the CNT arrays by preparing upside-down CNT films on different substrates. The CNT arrays on the growth substrates were lifted off by etching the Ni/TiN/SiO_2 layer and then transferred to TEM microgrids (or Si substrates) with their roots up, as shown in Fig. 2.7(a). we analyzed the bottom surface of a CNT array by XPS (Fig. 2.9) and confirmed that the Ni/TiN/SiO_2 layer was removed almost completely from the bottom surface. Such transfer was possible with minimal shrinkage of the film due to the solid nature of the CNT arrays as dense as ~1 g cm^{-3} (Fig. 2.8(a–d)) whereas was impossible for the CNT arrays with a lower density (0.3 g cm^{-3}) synthesized at 500 ℃ (Fig. 2.8(e,f)). Fig. 2.7(b) shows the SEM image of the CNT array transferred to the microgrid. The few-μm-wide cracks (A,B) were formed in the film by being torn and lifted up on one side, which match the counterpart remaining on the microgrid. The sub-μm-wide cracks (C,D) can also be seen, and these might originate from the shrinkage of the CNT arrays upon wetting and drying [65]. Overall, the transferred films showed minimal shrinkage (<few %) owing to the mass density being as high as ~1 g cm^{-3}. Fig. 2.7(c) shows an enlarged image of the lifted-up part of the CNT array in Fig. 2.8b. we can clearly see the upside-down structure in Fig. 2.7(c): rough top surface at the lower left side and smooth bottom surface at the upper right side. Fig. 2.8d–g shows the bottom-view SEM images of CNT arrays grown for 5 and 30 min. CNT roots are densely packed for the arrays grown for 5 min for both C_2H_2 pressures (Fig. 2.7(d,f)), whereas many voids were observed in the arrays grown for 25–

30 min for both C_2H_2 pressures (Fig. 2.7(e,g)). The increasing number of CNTs stop growing over time, and these are lifted up by the growing CNTs, resulting in the void formation at their root and decreasing mass density (Fig. 2.4(c)). When compared with the AFM image of the catalyst particles (Fig. 2.7(h)), the round shapes in the SEM images (Fig. 2.7(d–g)) seem somewhat larger. As discussed later using AFM images, the round shapes correspond to the roots not of the individual CNTs but CNT bundles in these SEM images.

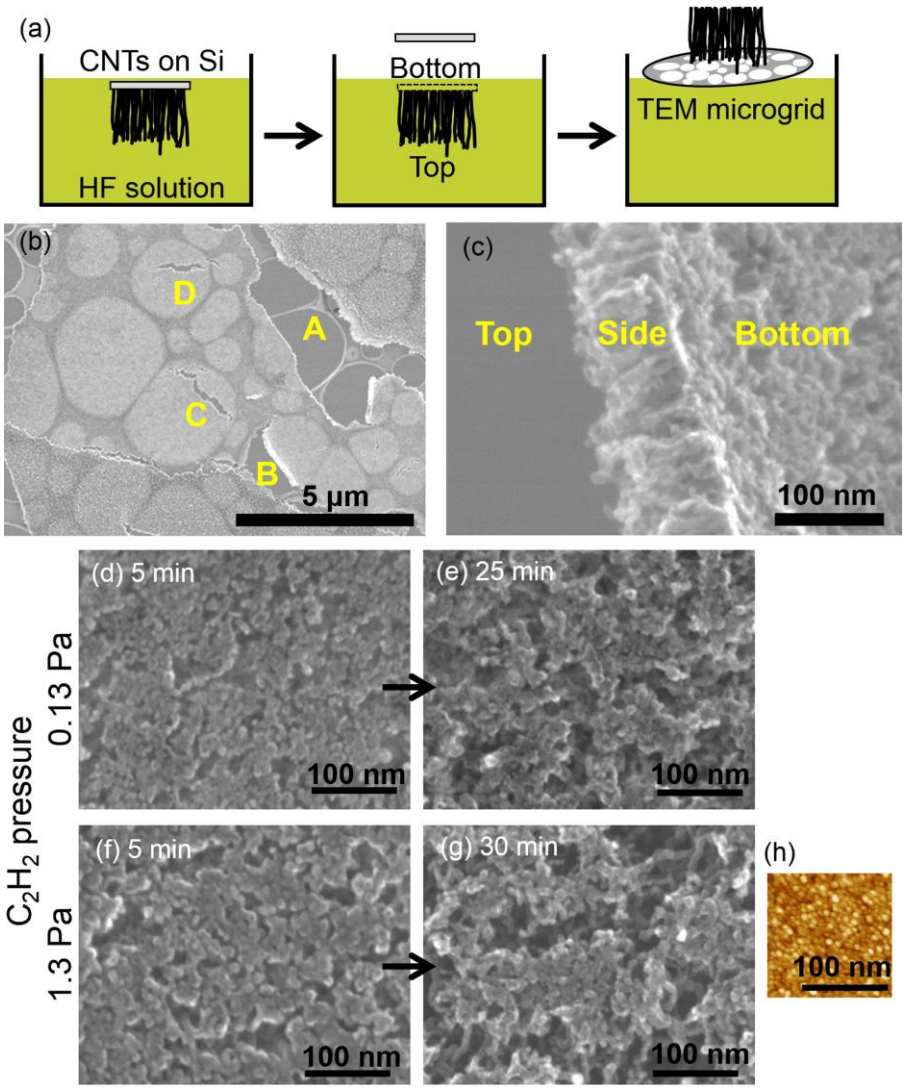

Fig. 2.7 (a) Schematic of the transfer process of the CNT arrays from the growth substrates to TEM microgrids; the Ni/TiN/SiO_2 layer in between the Si substrate and the CNT array was etched by HF (25 wt%) solution, and the CNT arrays floating in the solution were captured by the microgrid. (b,c) Typical SEM images of the CNT array transferred to the TEM microgrid. (d–g) High-magnification, bottom-view SEM images of the CNT arrays grown by Ni catalyst on TiN at 400 °C from (d,e) 0.13 and (f,g) 1.3 Pa C_2H_2 for (d,f) 5, (e) 25, and (g) 30 min. (h) The same AFM image of Ni catalyst particles as Fig. 2.3(e) is shown for comparison. The Ni particles were prepared under the same conditions as for Fig. 2.3(e) (400 °C and 8.1 pm s^{-1} with −20 V bias voltage) and used to grow the CNTs in (d–g).

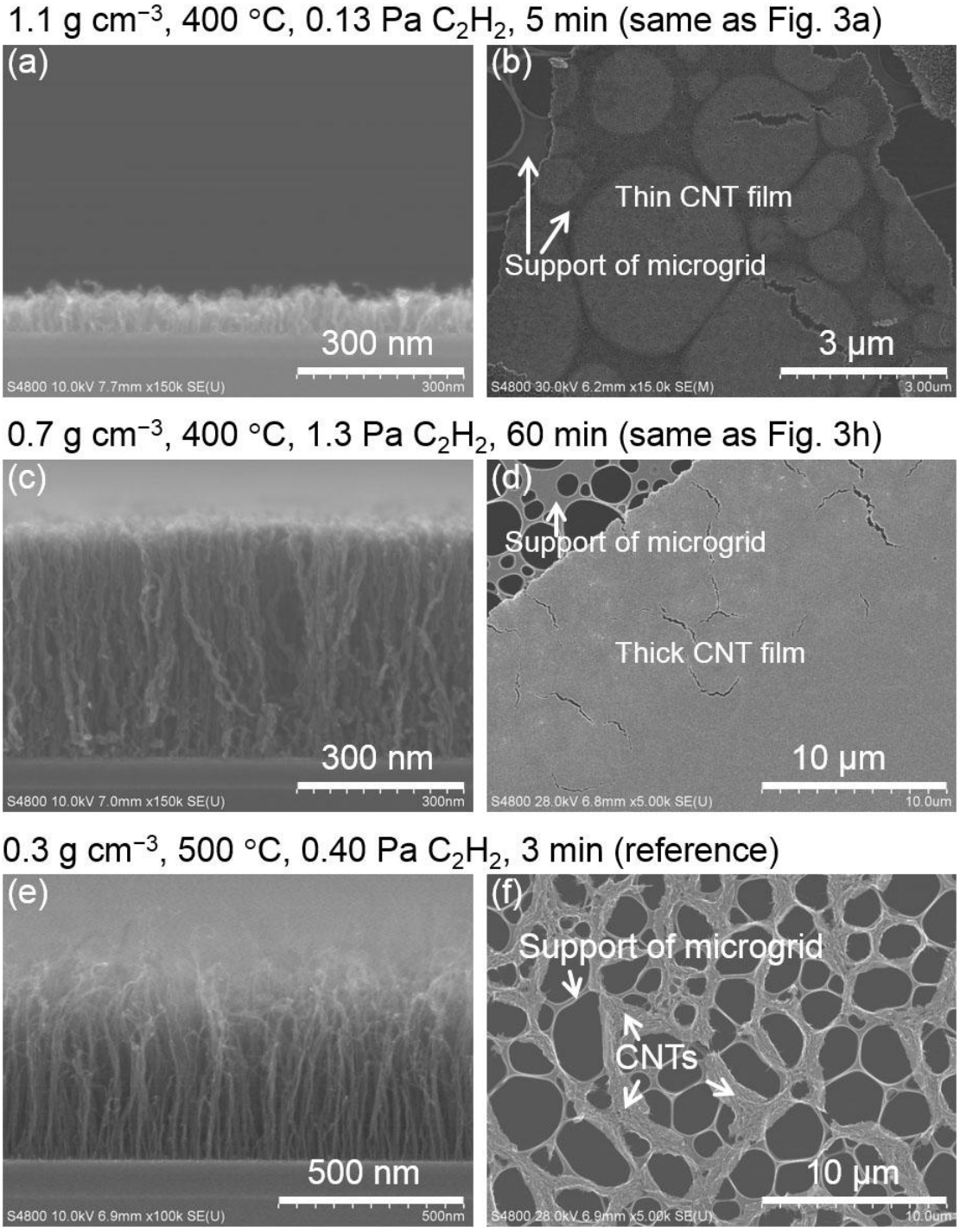

Fig. 2.8 Cross-sectional SEM images of as-grown CNT arrays (a,c,e) and plan-view SEM images of the CNTs transferred to microgrids (b,d,f) via the solution-based process shown in Fig. 2.7(a). The dense CNT arrays grown at 400 ℃ (a,c) kept the continuous film structure due to their solid nature (b,d) whereas the less-dense CNT arrays grown at 500 ℃ (e) shrank and broke into small pieces and wrapped the support of the microgrid (f).

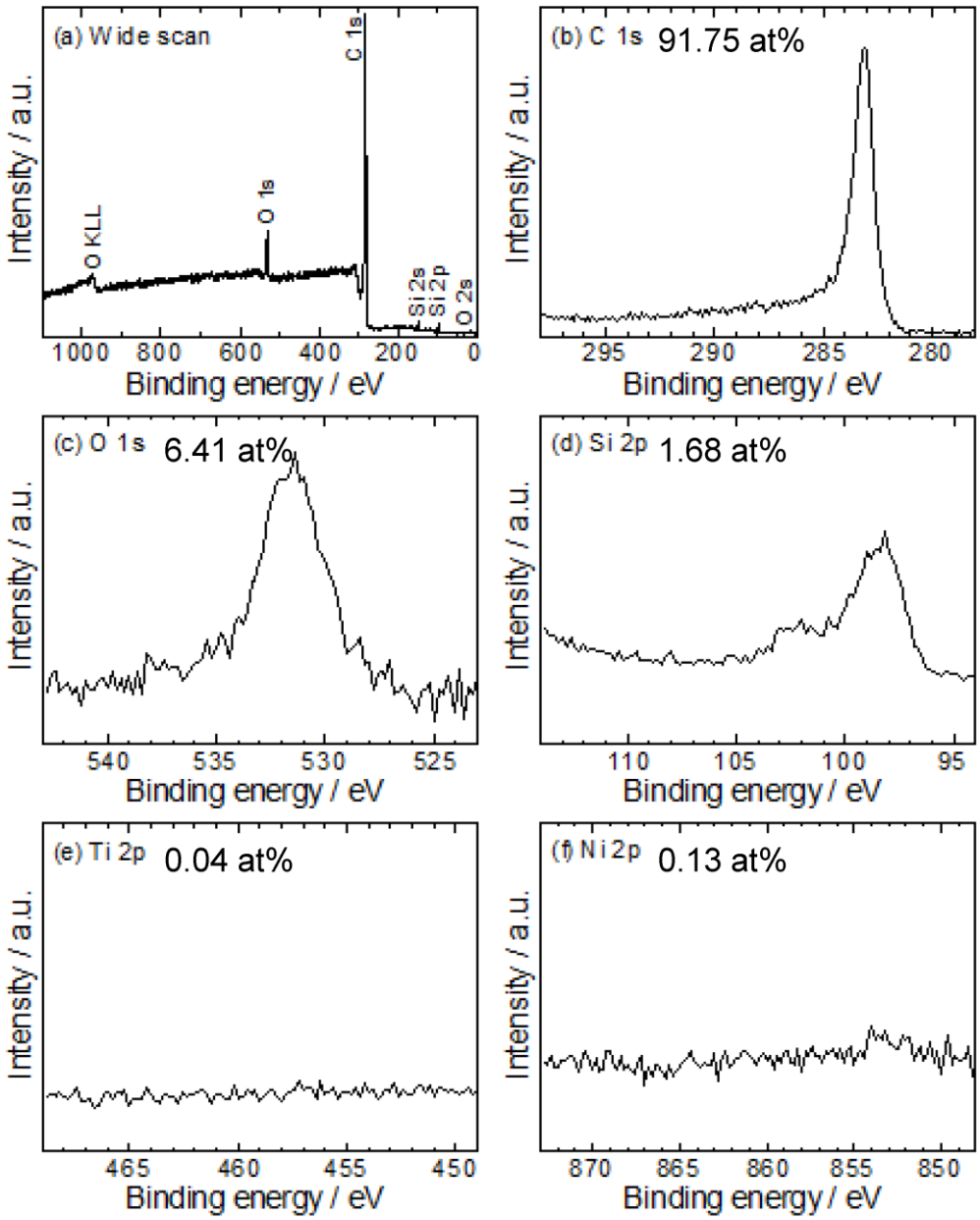

Fig. 2.9 XPS spectra and atomic concentration of the root of the CNT array transferred onto a Si substrate. The sample is the same as for Fig. 2.12.

Next, we carried out further analysis on the CNT arrays on the TEM microgrids using TEM (Fig. 2.10). To make electrons transmit through CNT arrays as dense as ~1 g cm^{-3}, the CVD time was adjusted to make CNT arrays as thin as ~100 nm (Fig. 2.10(a,c)). In the plan-view HRTEM images of the CNT arrays (Fig. 2.10(b,d)), densely packed concentric circles (shown by white arrows) can be seen, similar in appearance to the annual growth rings of trees,

corresponding to individual MWCNTs. Individual MWCNTs grown from 0.13 Pa (Fig. 2.10(b)) and 1.3 Pa (Fig. 2.10(d)) C_2H_2 were 7 and 8 nm in average diameter, respectively, and both had an average of 8 walls. The diameter and number of walls of individual CNTs were determined mainly by the structure of the catalyst particles used (Fig. 2.3(e)), although the CNT diameter may increase slightly with the increase in C_2H_2 partial pressure.

Growth of a CNT array at an intermediate C_2H_2 pressure (0.40 Pa) for 7 min was also investigated (Fig. 2.11). Their height and density, determined by SEM and EDS analyses (Fig. 2.11(a,b)), were approximately 140 nm and 1.1 g cm^{-3}, respectively, which are similar but somewhat taller and denser than the CNT array grown at 0.13 Pa for 10 min (Fig. 2.6). we carefully analyzed the root of this CNT array by bottom-view AFM (Fig. 2.11(c–e)). The low-magnification image (Fig. 2.11(c)) shows that the film had the densely packed region at 92% with the void regions at 8%, which may have been caused by the solution-base transfer process discussed for Fig. 2.7. The densely packed regions (Fig. 2.11(d,e)) were observed at a higher magnification, which provides the clear image of the roots of individual CNTs. The number of CNTs were 1.7×10^{12} cm^{-2} (Fig. 2.11(d)) and 1.6×10^{12} cm^{-2} (Fig. 2.11(e)). By considering the coverage of the densely packed region (92%), we determined the number density of CNTs for the whole region to be 1.5×10^{12} CNTs cm^{-2}. The number of walls in individual CNTs were eight for CNTs grown at both 0.13 and 1.3 Pa C_2H_2 (Fig. 2.10) and, thus, we conclude the number density of CNT walls to be 1.2×10^{13} walls cm^{-2}. Fig. 2.11(g) schematically shows the CNT structure determined, in which the surface coverage of CNTs is as high as 58%. By using typical values for CNTs (7-nm diameter for the outermost wall, 0.35-nm radial interspacing between the walls, and 1.5×10^{12} CNTs cm^{-2} number density), we can calculate the mass density of the CNT array to be 1.25 g cm^{-3}, which is close to and, thus, consistent with the

density determined by SEM-EDS. However, the number density of CNTs (1.5×10^{12} CNTs cm^{-2}) is about half that of the catalyst particles (2.8×10^{12} cm^{-2}, Fig. 2.3(e)) owing to the imperfect nucleation of CNTs and gradual deactivation of the catalyst particles during CVD. Therefore, there remains room for further enhancement of the CNT wall density beyond 2×10^{13} cm^{-2}.

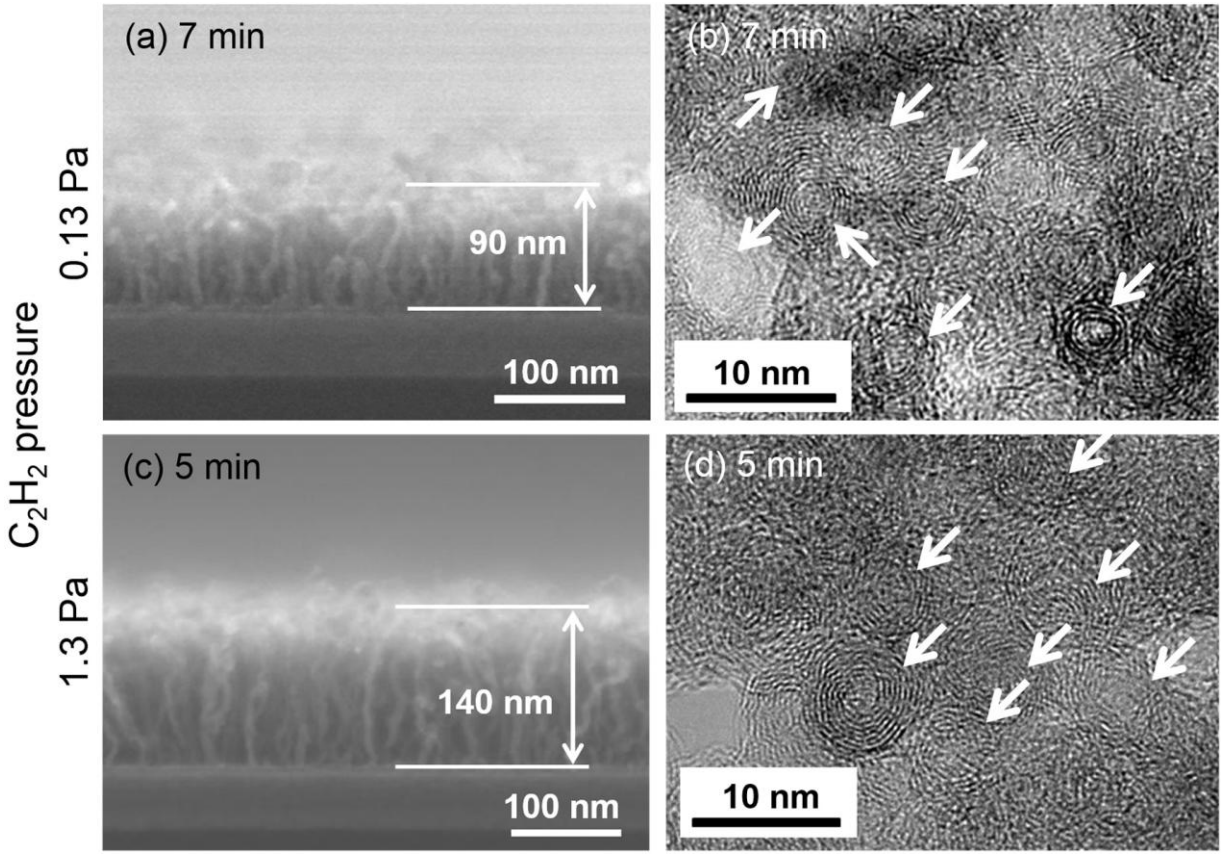

Fig. 2.10 Cross-sectional SEM (a,c) and plan-view HRTEM (b,d) images of the CNT arrays grown at 400 ℃ from 0.13 (a,b) and 1.3 (c,d) Pa C_2H_2 using the Ni/TiN catalyst under the same conditions as in Fig. 2.3(e) (400 ℃, 8.1 pm s^{-1}, and −20 V bias voltage). The CNT arrays were transferred to the TEM microgrids by the method shown in Fig. 2.7.

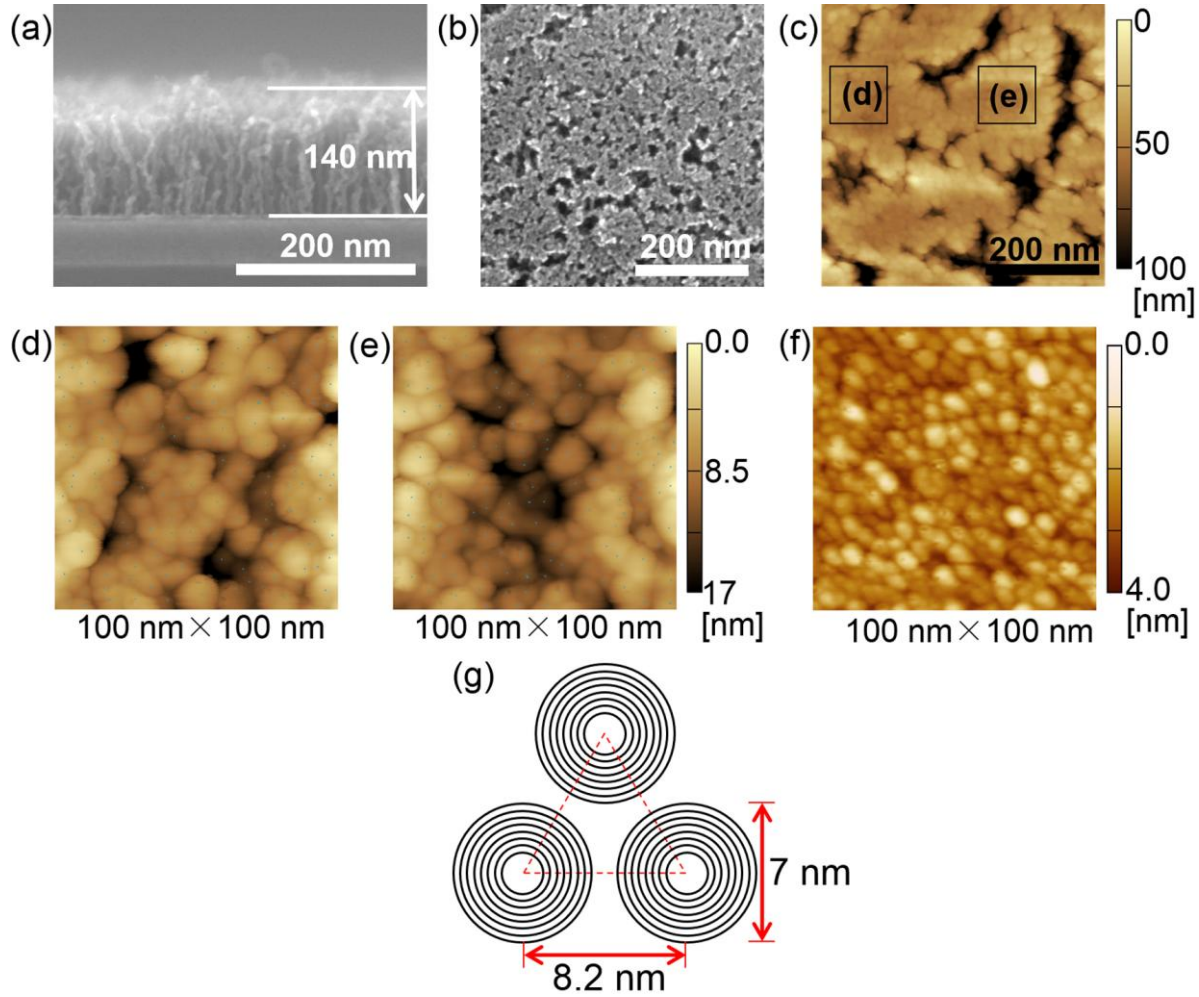

Fig. 2.11 Cross-sectional SEM image of the CNT arrays on the growth substrate (a), and (b) bottom-view SEM and (c) AFM images of the same CNT arrays transferred to another Si substrate. The CNT arrays were grown at 400 ℃ from 0.40 Pa C_2H_2 for 7 min using the Ni/TiN catalyst under the same conditions as for Fig. 2.3(e) (400 ℃, 8.1 pm s^{-1}, and −20 V bias voltage). (d,e) High-resolution AFM images of the CNT roots, corresponding to positions (d) and (e) shown in (c). (f) The same AFM image as Fig. 2.3(e) is shown at the same scale as (d,e) for comparison. (g) A schematic of the CNT structure in the array with the CNT number density of 1.5×10^{12} cm^{-2}, an average CNT diameter of 7 nm, and number of CNT walls of eight.

2.3.4 Electrical conductivity measurement of the dense CNT arrays

we performed some characterization of quality and resistance of the CNTs. HRTEM images of individual CNTs were taken for the CNT arrays (Fig. 2.12). The dense (0.7 g cm^{-3}) array

synthesized at 400 ℃ (Fig. 2.12(a)) was comprised of rather defective CNTs (Fig. 2.12(b)) whereas the less dense (0.3 g cm^{-3}) array synthesized at 500 ℃ (Fig. 2.12) was comprised of less defective CNTs (Fig. 2.12(d)). These results show that the growth of individual CNTs gets much easier for a temperature increase by 100 ℃. Current-voltage curves for various samples were evaluated by AFM using a conductive tip with a curvature radius of R = 25 nm (Fig. 2.13). we obtained resistance values of 39–95 kΩ for CNTs grown at 400 °C, which are comparable with the previous works; 95 ± 46, 35, 80 ± 60 kΩ for CNTs grown at 450, 475, 650 °C using AFM tips with R = 20, 20–30, ~20 nm, respectively [58, 66, 67]. The resistance values should be affected by the contact resistance between the AFM tip and the CNT arrays, which could be reduced by forming appropriate contact layer [54]. How to improve the quality of CNTs at low CVD temperature as well as how to build a good electrical contact with CNT tips are remaining issues.

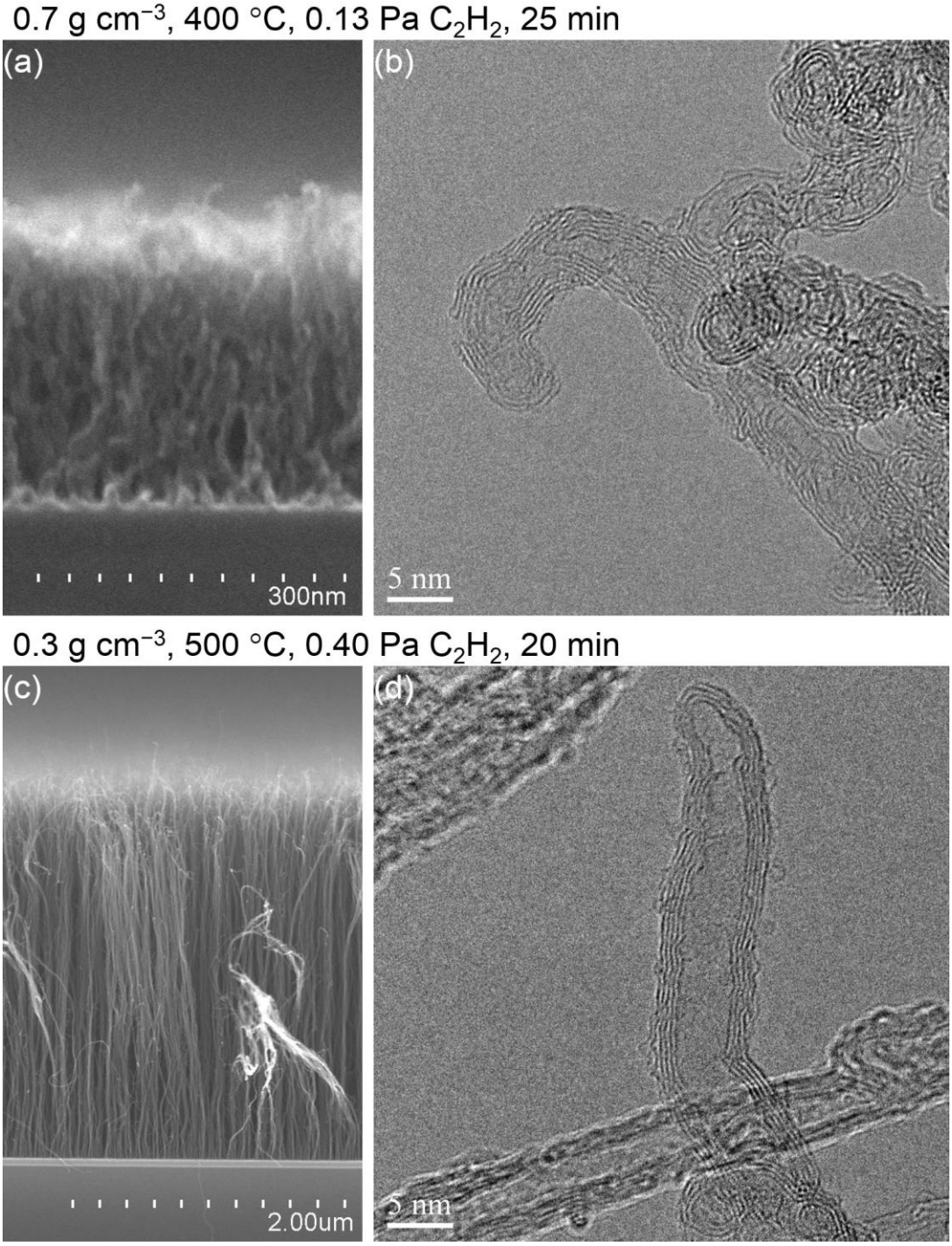

Fig. 2.12 Cross-sectional SEM images of the CNT arrays (a,c) and HRTEM images of individual CNTs in the arrays (b,d). The dense array synthesized at 400 ℃ (a) was comprised of rather defective CNTs (b) whereas the less dense array synthesized at 500 ℃ (c) was comprised of less defective CNTs (d). The growth of individual CNTs gets much easier for a temperature increase of only 100 ℃.

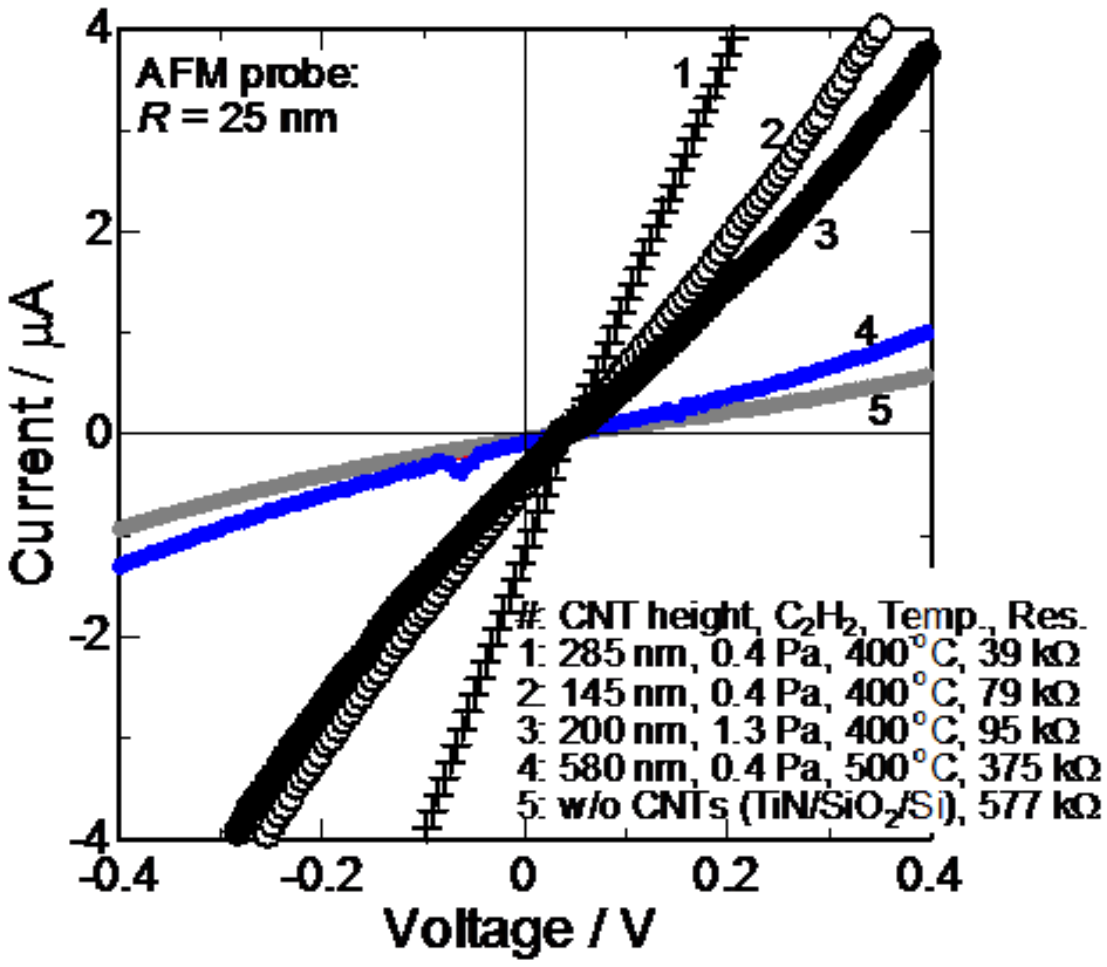

Fig. 2.13 Current-voltage curves for various samples evaluated by AFM using a conductive tip with a curvature radius of R = 25 nm. The growth conditions and the resulting CNT heights were shown in the graph. CNTs grown at 500 ℃ are also shown for comparison. For the sample w/o CNTs, a 5-nm-thick TiN was deposited on SiO_2/Si substrate and then annealed in H_2/Ar at 400 ℃ without carrying out CVD. An off-set of ~0.04 V as well as some curvature similar to [66, 67] were observed. The resistance values were obtained by fitting the linear region between −0.1 and 0.2 V. These resistance values of 39–95 kΩ for CNTs grown at 400 ℃ (#1–3) are comparable with the previous works; 95 ± 46, 35, 80 ±60 kΩ for CNTs grown at 450, 475, 650 ℃ using AFM tips with R = 20, 20–30, ~20 nm, respectively [58, 66, 67]. The resistance values should be affected by the contact resistance between the AFM tip and the CNT arrays, which could be reduced by forming appropriate contact layer [54]. The resistance values were smaller for CNTs grown at 400 ℃ than for CNTs at 500 ℃ and w/o CNTs, suggesting the improved electrical contact between the TiN layer and the AFM tip by the CNTs grown at 400 ℃.

2.4 Conclusions

To realize the practical application of CNTs, requirements for both structure and process need to be satisfied. For via interconnects in LSIs, CNTs need to be prepared at high density (~10^{13} walls cm^{-2}) and at low temperature (≤ 400 °C) on a conductive underlayer. we propose a simple process for the preparation of dense catalyst particles through their nucleation and growth during conventional sputter deposition on device substrates but with carefully engineered conditions to control the moderate initial island density. we prepared moderately dense Ni islands on a conductive TiN layer by lowering the deposition rate to 8.1 pm s^{-1}, heating the substrate to 400 ℃, and applying a −20 V bias voltage to the substrate. This led to a retained Ni particle density as high as 2.8 × 10^{12} cm^{-2} after annealing at 400 ℃. we also proposed a simple process for CNT growth by conventional thermal CVD without using plasma but with carefully engineered conditions: low temperature of 400 ℃ with a low C_2H_2 pressure of 0.13–1.3 Pa so as not to kill the catalyst.

From SEM-EDS analysis, we found that the 100- to 300-nm-tall CNT arrays had a mass density as high as ~1 g cm^{-3}. We proposed and developed a new simple method to directly count the number of CNTs in the array, simply by transferring CNTs to a different substrate (TEM microgrids or Si substrates) with their roots up and by taking the plan-view HRTEM and bottom-view AFM images. Through these analyses, we found that Ni catalyst particles at 2.8 × 10^{12} cm^{-2} grew CNTs at 1.5 × 10^{12} CNTs cm^{-2} and 1.2 × 10^{13} walls cm^{-2}. Such CNTs, formed on a conductive TiN layer at a maximum process temperature of just 400 ℃ using conventional sputtering and CVD apparatus, and showing electric conduction with resistance of few-tens kΩ to the TiN underlayer by AFM measurement, would be suitable for the practical application of CNTs to via interconnects in LSIs.

Chapter 3 - Tens-Micrometer-Tall, High-Density CNT Arrays on Both Sides of Cu foils for TIMs

1.1 Introduction

Carbon nanotubes (CNTs) have attracted great attention due to their unique one dimensional nanostructure and various characteristic properties including excellent electric and thermal conductivities in their axial direction [40]. Vertically aligned CNT (VA-CNT) arrays are thus ideal when we consider their possible applications such as interconnects in ultra-large scale integrated circuits (ULSIs) [30, 68] and thermal interface materials (TIMs) [38]. VA-CNT arrays were first reported for multi-wall CNTs (MWCNTs) by chemical vapor deposition (CVD) using Fe catalysts supported on mesoporous silica [32, 33]. Several years later, such growth were reported for single-wall CNTs (SWCNTs) using Co-Mo catalysts [41] and Fe/Al_2O_3

catalyst [14, 42, 49] supported on flat substrates of quartz glass or SiO_2/Si. Extensive efforts have been made and such growth is now possible for SWCNTs, double-wall CNTs (DWCNTs), and MWCNTs with fairly high areal densities of 10^{10}–10^{12} CNTs cm^{-2}. Such "superdense and vertically aligned nanotube forests" [33], however, are mainly composed not of CNTs but of air, as later been reported as "a very sparse material where SWNTs represent only 3.6% of the total volume" [49].

We made a systematic survey on the type, height, and mass density of CNT arrays and found a general tradeoff between the mass density and height of the CNT arrays. Fig. 3.1 summarizes the mass density and height of the arrays in previous reports [42, 49, 57, 58, 69-77] and the present work, which clearly shows the tradeoff regardless of the type of CNTs (i.e. SWCNTs, DWCNTs, and MWCNTs) for a wide range; very high mass density ~ 1 g cm^{-3} for short arrays of sub μm whereas very low mass density < 0.1 g cm^{-3} for tall arrays > 100 μm (and even 0.003 g cm^{-3} for a 400-μm-tall MWCNT array). Because air is insulating both for electrical and thermal conductions, growing VA-CNTs at high mass densities is a key issue for their practical use in such conductivity enhancement.

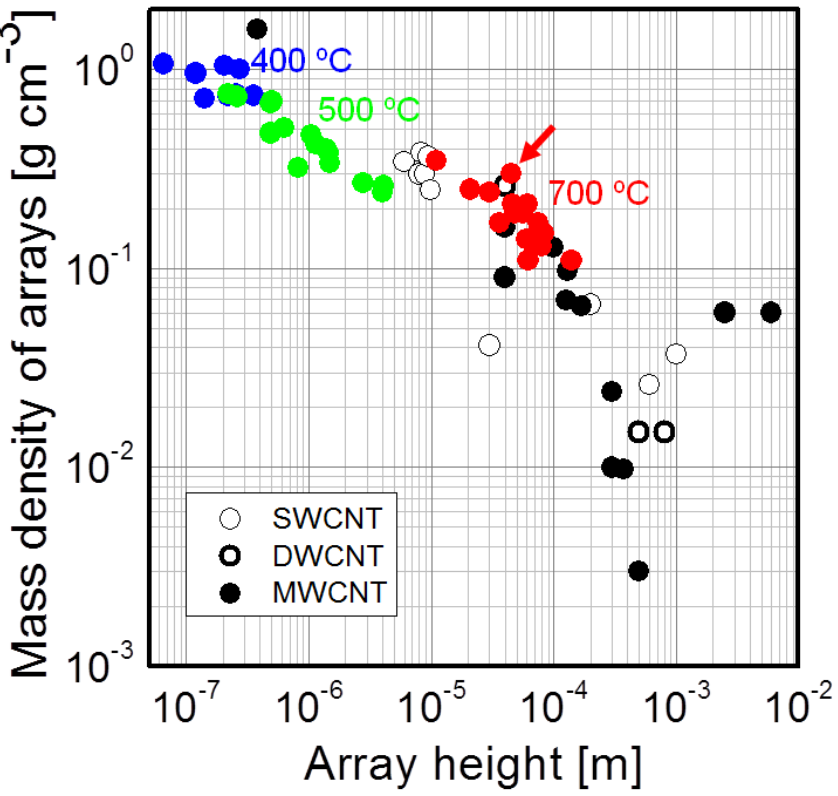

Fig. 3.1 Tradeoff appearing in the height and mass density of VA-CNT arrays grown on insulating [42, 49, 57, 58, 69-77] and conductive [58] underlayers. Values from previous reports [42, 49, 57, 58, 69-77] are shown in black symbols with corresponding reference numbers. Results of the present work on conductive underlayers are shown in solid circles in color; blue at 400 ℃ using Ni catalyst on $TiN/SiO_2/Si$, green at 500 ℃ using Ni catalyst on $TiN/SiO_2/Si$, and red at 700 ℃ using Fe catalyst on TiN/Ta/Cu.

The progress in CNT growth technology and the increasing demand for thermal management in electronic devices motivated researchers to use CNT arrays for TIMs [31, 78-81]. Such TIMs can be categorized into three types; (I) CNT arrays directly on the surface of either the heat source or heat sink, (II) those directly on both the surfaces of the heat source and heat sink, and (III) metal foils with CNT arrays on both faces which are inserted between the heat source and heat sink, as summarized in Tables 3.1 and 3.2. Very recently, TIMs of high density CNT arrays (40 μm in height and 0.27 g cm^{-3}) bonded to both Si chip and heat sink using indium was also reported [77]. Type III is inferior in thermal resistance than the others because of the greater number of interfaces in the structure (i.e., four interfaces of heat

source/CNT/foil/CNT/heat sink for the former vs. two interfaces between the heat source/CNT/heat sink for the latter). However, Type III is superior in avoiding any thermal damage to the electronic chips and easiness in their use, just putting them between electronic chips and heat sinks. Cu foils are inexpensive, possess excellent thermal conductivity, and have sufficiently high melting point compared with the typical CVD temperatures (600–800 ℃). Using diffusion barriers (mainly AlO_x [31, 82, 83]) which prevent catalysts from deactivation in the reaction with Cu, several groups have realized the growth of CNT arrays to several tens of μm in height. When we consider the electrical conduction, growing CNTs on conductors such as TiN/Ta/Cu [55], Mo/Ti/Cu [58], and Au/Cr/Cu [84] is also essential, however such growth is still very rare for several tens of μm-tall CNT arrays.

In this work, toward wide use of VA-CNTs, we worked on growing denser and taller CNT arrays using conductive underlayer on Cu foils. We first studied a range of catalysts (Fe, Co, Ni) and CVD conditions (400–700 ℃ and 0.40–27 Pa C_2H_2) to produce several tens of μm-tall CNT arrays. C_2H_2 is known to be an efficient direct growth precursor [16], and the control of its partial pressure is known to be crucial for achieving CNT growth at different temperatures [11, 34]. Next, we applied TiN and Ta layers, which are known effective conductive underlayers [55], to Cu foils, optimized their thickness, and clarified their roles. Finally, we fabricated CNT/Cu/CNT TIMs with controlled mass density of the CNT arrays. Despite of the importance of the surface roughness of the contacting materials on the thermal resistance, there is little quantitative information available on features such as average surface roughness (Ra) and average peak-to-valley surface height (Rz) [31, 81]. Typical heat sources and heat sinks often have surface roughness of several tens of μm and thus we evaluated their thermal resistance with metal blocks having surface roughness of 20−30 μm.

Table 3.1 Thermal resistance between a CNT-grown Si surface and a counter solid surface.

Type	Si surface [a]	Counter surface [a]	Thermal resistance	Ref.
I	CNT/Fe/Ti/SiO_2/Si (roughness: N/A)	Ag foil (25 μm) (roughness: N/A)	11−18 mm^2 K W^{-1} at 0.07 MPa 8−19 mm^2 K W^{-1} at 0.21 MPa	[78]
I	CNT/Fe/SiO_2/Si (roughness: N/A)	Ni (100 nm)/ZnSe (roughness: N/A)	8−26 mm^2 K W^{-1} at 0.41 MPa	[79]
I	CNT/Ni/Al/Ti/SiO_2/Si (roughness: N/A)	Al alloy plate (roughness: N/A)	7 mm^2 K W^{-1} at 0.15 MPa	[80]
I	CNT/Ni/Al/Ti/Si (R_a = 0.01 μm, R_z = 0.09 μm)	Ag foil (R_a = 0.06 μm, R_z = 0.4 μm)	15.8±0.9 mm^2 K W^{-1} at 0.24 MPa	[81]
II	CNT/Ni/Al/Ti/Si (R_a = 0.01 μm, R_z = 0.09 μm)	CNT/Ni/Al/Ti/Cu (R_a = 0.05 μm, R_z = 0.5 μm)	4.1±0.4 mm^2 K W^{-1} at 0.17 MPa 4.0±0.4 mm^2 K W^{-1} at 0.24 MPa	[81]

[a] Roughness is shown for the base substrate.

Table 3.2 Thermal resistance between two solid surfaces connected with a CNT/Cu/CNT TIMs.

Type	Catalyst	One surface	Another surface	Thermal resistance	Ref.
III	Fe/ Al 10 nm/ Ti 30 nm	Si (R_a = 0.01 μm, R_z = 0.09 μm)	Ag foil (R_a = 0.06 μm, R_z = 0.4 μm)	14 mm^2 K W^{-1} at 0.07 MPa 8 mm^2 K W^{-1} at 0.28 MPa	[31]
III	Fe/ Al 10 nm/ Ti 30 nm	Cu (R_a = 2.8 μm, R_z = 9.3 μm)	Ag foil (R_a = 0.06 μm, R_z = 0.4 μm)	18 mm^2 K W^{-1} at 0.07 MPa 12 mm^2 K W^{-1} at 0.28 MPa	[31]
III	Fe from ferrocene	Cu block (roughness: N/A)	Cu block (roughness: N/A)	12 mm^2 K W^{-1} at 0.3 MPa	[84]

3.2 Experimental

3.2.1 Catalyst preparation and CNT growth

The same apparatuses as that described in our previous report [34] were used for catalyst deposition, CNT growth, and characterization of the obtained catalysts and CNTs. 99-wt%-pure Cu foils (Nilaco, Tokyo, Japan) of 20, 50, and 80 μm in thickness and Si wafers with 50-nm-thick SiO_2 layer were used as substrates for the TIMs and structural analyses, respectively. The Cu foils were cleaned using isopropyl alcohol followed by annealing at 1000 ℃ under a flow of 4 kPa H_2 for 10 min. Then, 0–30-nm-thick Ta and 0–30-nm-thick TiN layers were successively deposited on the Cu foils. Finally, the selected catalysts (Fe, Ni, Co) were deposited on the TiN/Ta/Cu structures. All deposition processes were carried out by magnetron sputtering with three 2-inch targets (ULVAC MPS-2000HC2S, Chigasaki, Japan) without breaking the vacuum. Comparison of the catalysts revealed Fe to be the most effective for growing CNTs of several tens of μm in height at 700 ℃, and thus various deposition conditions were investigated for it, including temperature (room temperature (R.T.) and 400 ℃), deposition rate (63 and 22 pm s^{-1}), and substrate bias (0 and –20 V). The deposition rate was controlled by varying the Fe target discharge power between 20 and 100 W. Samples were set in a tubular quartz glass CVD reactor, and annealed during heating to and holding for 8 min at 400 and 500 ℃, or 3 min at 600, 700, and 800 ℃ under a flow of 4 kPa H_2. Then, CNTs were grown for 3–30 min under C_2H_2 (0.4–26.7 Pa) and H_2 (0, 0.27 kPa) with Ar balance at a total pressure of 2 kPa. CNTs were also grown on both faces of Cu foils for thermal measurements.

3.2.2 Characterization of catalyst and CNT structures

The number densities of catalyst particles obtained after the annealing step were determined by atomic force microscopy (AFM; Shimadzu SPM 9600, Kyoto, Japan). Surface elemental compositions were examined by X-ray photoelectron spectroscopy (XPS; JEOL JPS9010 TR, Akishima, Japan) for the as-deposited and annealed samples. Ta and TiN/Ta underlayers were also formed in SiO2/Si (100) substrates and characterized by in-plane X-ray diffraction (XRD; Rigaku RINT Ultima III, Akishima, Japan) using Kα radiation (λ=1.54 Å) for their crystal structures and by the four-point-probe method for their conductivities. The CNTs were characterized by field emission scanning electron microscopy (FE-SEM; Hitachi S-4800, Tokyo, Japan). Some CNTs were characterized by high-resolution transmission electron microscopy (HRTEM; JEM-2100F; JEOL, Akishima, Japan) by transferring them to a TEM microgrid using tweezers. Each sample was weighed before and after CVD using a microbalance with a sensitivity and precision of 1 μg. The CNT mass densities of the samples were obtained by measuring the heights of the grown CNTs and weight changes of the samples.

3.2.3 Thermal resistance evaluation

A thermal tester (Mentor Graphics T3Ster1.1C, Wilsonville, OR, USA) was used to evaluate the thermal resistance of the samples between Cu and Al blocks at a pressure of 0.34 MPa. A CNT/Cu/CNT TIM was mounted on the Al block base, the Cu block with a semiconductor power chip embedded inside was mounted on the CNT/Cu/CNT TIM, and the pressure was applied to the stack. The semiconductor power chip was used as both the heat source and the temperature sensor (based on the temperature dependent PN junction property or the threshold

voltage). Measurement was carried out by an on/off operation of 1.6 W input power with a measurement delay time of 30 s. Power input and temperature monitoring were controlled by the T3Ster thermal tester, and the transient temperature was analyzed by it to derive the thermal characteristics of the test structure. The surface roughness of these blocks was evaluated using three-dimensional (3D) laser scanning microscope (VK-X200, Keyence, Osaka, Japan). Both blocks had rough surfaces; R_a = 1.8 μm and R_z = 21.3 μm for the Cu block, and R_a = 2.0 μm and R_z = 27.3 μm for the Al block (Fig. 3.2). The measurable thermal resistance range was ca. 2–1000 mm^2 K W^{-1}.

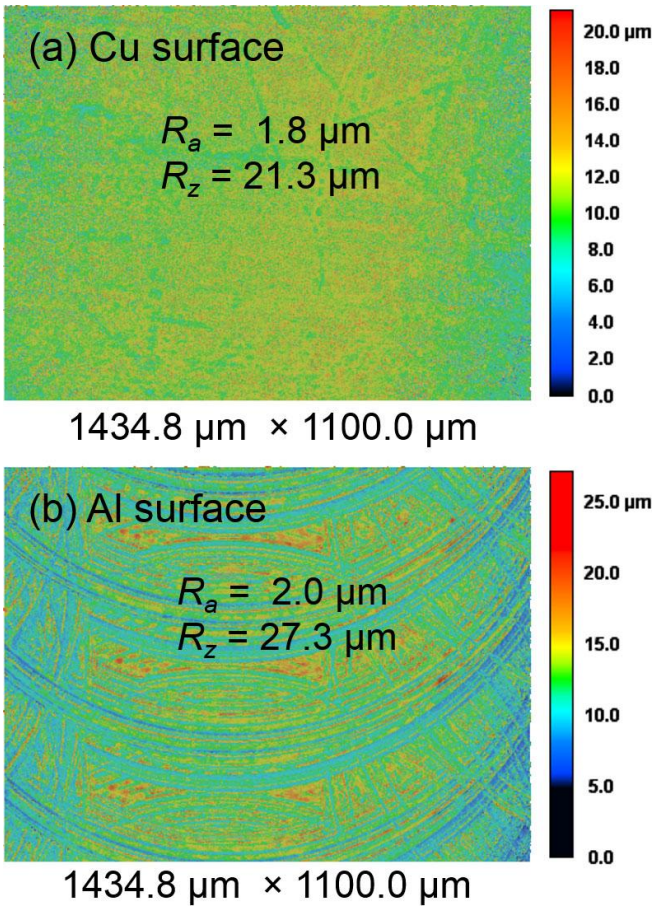

Fig. 3.2 3D laser scanning microscope images of the metal blocks used for the thermal resistance measurement. Both blocks had rough surfaces; R_a = 1.8 μm and R_z = 21.3 μm for the top Cu block (a), and R_a = 2.0 μm and R_z = 27.3 μm for the bottom Al block (b).

3.3 Results and discussion

3.3.1 Comparison of catalysts for CNT array growth

We previously reported the fabrication of high-density CNT arrays (mass density: 1.1 g cm^{-3}, wall density: 1.2×10^{13} cm^{-2}) targeting at via interconnects in ULSIs [34], but their height (sub μm) was limited owing to the low growth temperature used (400 °C). Therefore, we first investigated the growth conditions required to produce several tens-μm-tall CNT arrays. Fig. 3.3 shows the heights of CNT arrays grown using Fe, Co, and Ni catalysts on TiN/SiO_2/Si at different C_2H_2 pressures and CVD temperatures (600, 700, and 800 ℃) for 30 min. Co showed the highest catalytic activity at 600 ℃, yielding 59-μm-tall CNT arrays from 13 Pa C_2H_2. In contrast, Fe was the most catalytically active at 700 ℃, yielding the tallest CNT arrays (96 μm) from 27 Pa C_2H_2. However, further increase in temperature to 800 °C resulted in very short (~3 μm) arrays, possibly owing to reaction of the Fe with the TiN underlayer.

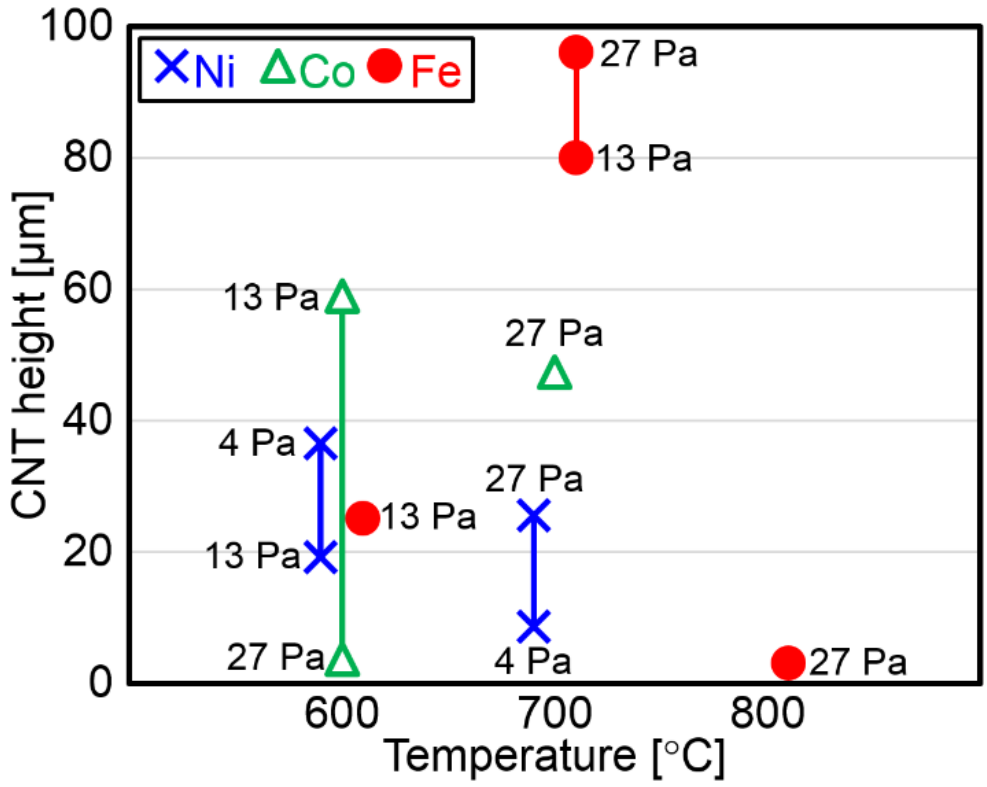

Fig. 3.3 Heights of CNT arrays grown in 30 min by CVD on TiN (5 nm)/SiO_2/Si using Fe (1.0 nm), Co (0.8 nm), and Ni (0.6 nm) catalysts at different C_2H_2 pressures and temperatures (600, 700, 800 ℃). The inset values show the C_2H_2 pressures. The x-positions are slightly shifted to the left and right for Ni and Fe, respectively, to be easily seen. The catalyst and underlayer were deposited at R.T.

We then compared the growth of CNT arrays on SiO_2/Si substrates and Cu foils (Fig. 3.4). On TiN/SiO_2/Si, Ni showed good catalytic activity at low temperatures of 400 and 500 ℃, but the array height was limited to a few μm (Fig. 3.4(a,b)). Fe showed good catalytic activity at a high temperature of 700 ℃ (Fig. 3.4(c)). These results show that the TiN layer was effective in maintaining catalyst activity between 400 and 700 °C. In contrast, on TiN/Cu, wavy, short CNT arrays grew at 400 °C (Fig. 3.4(d)), and no CNTs grew at 500 or 700 °C (Fig. 3.4(e,f)). Thus, the catalyst particles were easily deactivated by Cu but not by TiN. The addition of a Ta layer between TiN and Cu had a drastic effect; CNT arrays formed under all conditions (Fig. 3.4(g–i)) and their height reached 22 μm using the Fe catalyst at 700 °C (Fig. 3.4(i)). However, the CNT

arrays on TiN/Ta/Cu were still shorter than those obtained on SiO_2/Si, especially for higher growth temperatures. We therefore decided on using the Fe catalyst, a CVD temperature of 700 °C, and examined the effect of the TiN and Ta underlayers in the following experiments.

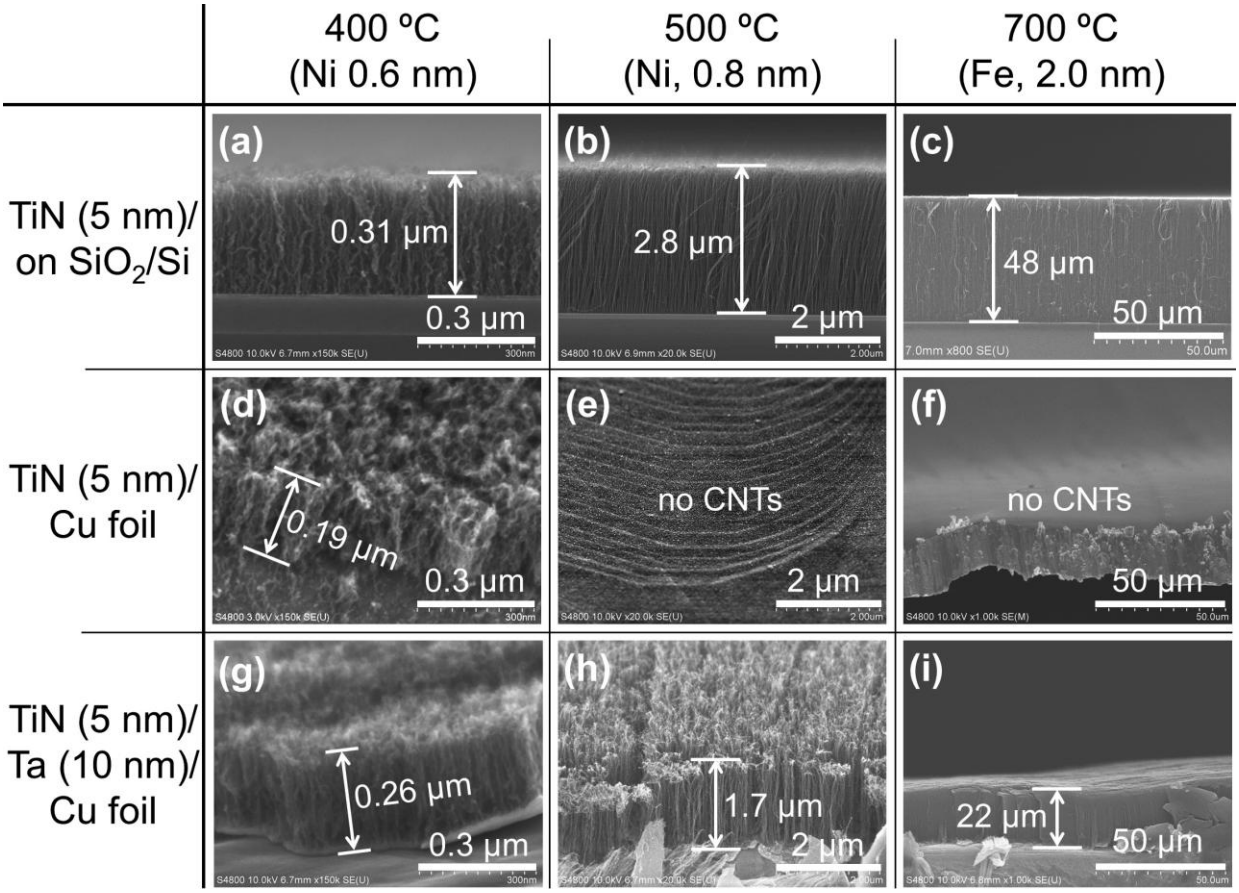

Fig. 3.4 SEM images of CNT arrays grown on various underlayer/substrate combinations using various temperature-catalyst conditions. The C_2H_2 pressure and growth time were 0.4 Pa and 20 min for (a,b,d,e,g,h) and 26.7 Pa and 30 min for (c,f,j), respectively. The catalyst and underlayers were deposited at R.T.

3.3.2 Catalyst underlayers for CNT array growth on Cu foils

Fig. 3.5 shows the CNT arrays grown on Cu foils with TiN and Ta underlayers of different thicknesses at 700 ℃ and 27 Pa C_2H_2. Without a TiN underlayer, the CNTs grew in a randomly aligned array with a height of a few μm (Fig. 3.5(b)), showing that TiN is essential as an

underlayer for the Fe catalyst to achieve CNT growth on Ta/Cu. A Ta layer was also needed as discussed for Fig. 3, but the CNT growth was not so sensitive to the Ta layer thickness (Fig. 3.5(a,c,e)). We selected TiN (15 nm)/Ta (10 nm)/Cu as the standard condition (Fig. 3.5(c)), which yielded the tallest CNT arrays with high density (70 μm, 0.21 g cm^{-3}).

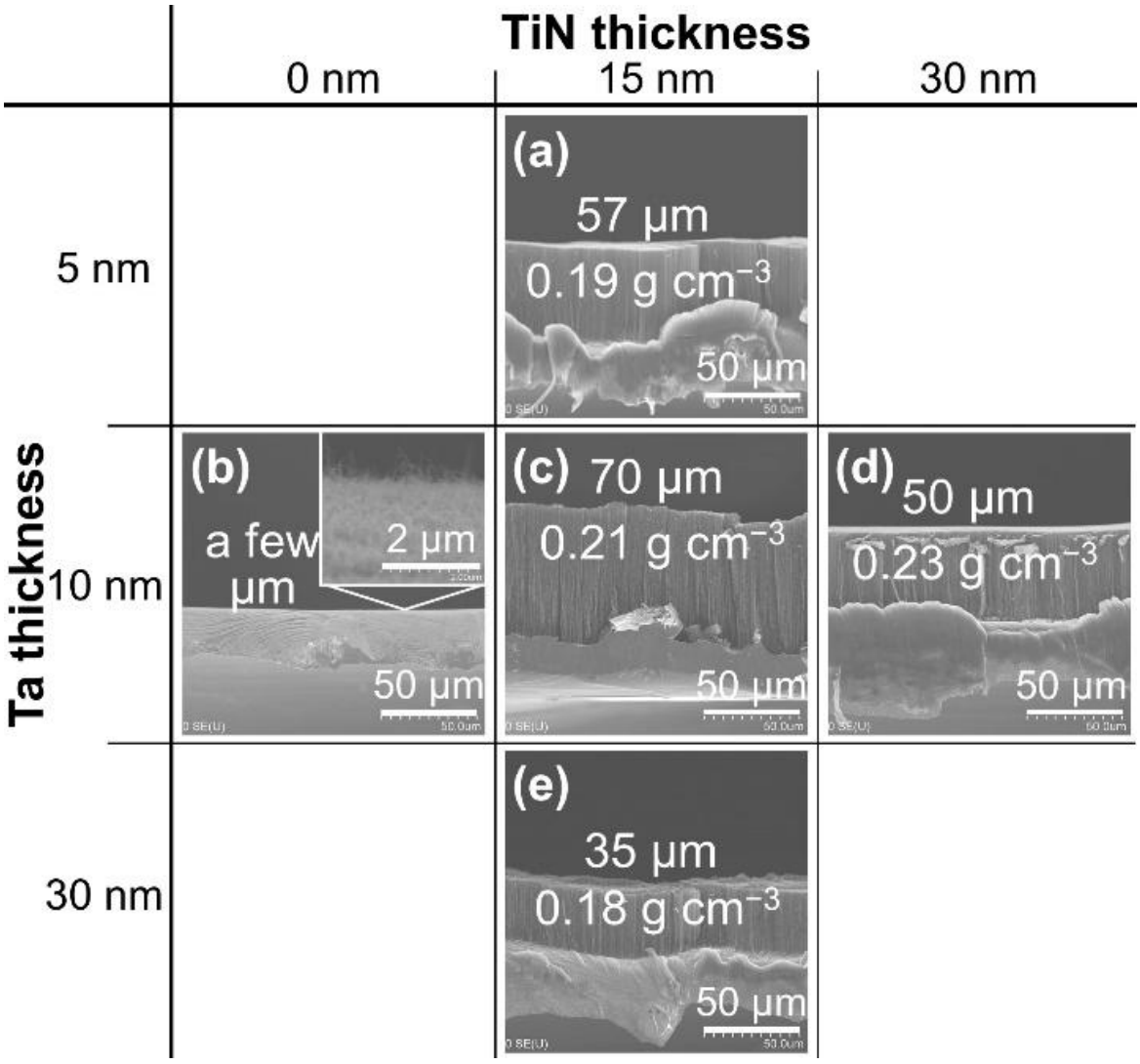

Fig. 3.5 Cross-sectional SEM images of CNT arrays grown on Cu foils with different TiN (0, 15, 30 nm)/Ta (5, 10, 30 nm) underlayers using Fe (2 nm) and 27 Pa C_2H_2 at 700 °C for 30 min. The catalyst and underlayers were deposited at R.T.

We examined the role of the underlayers by analyzing the surface elemental composition of the as-deposited and annealed samples by XPS (Fig 3.6). For the standard as-deposited Fe (2.0

nm)/TiN (15 nm)/Ta (10 nm)/Cu samples (Fig. 3.6(a–d)), a strongx Fe peak and weak Ti peak were observed but no Ta and Cu peaks were observed, confirming the formation of the layered structure. After annealing at 700 °C, the Fe peak became very weak (Fig. 3.6(e)) and the Cu peak became very strong (Fig. 3.6(h)) without the Ta layer (orange curves), whereas Fe peak remained strong (Fig. 3.6(e)) and the Cu peak remained weak (Fig. 3.6(h)) with the Ta layer (black and red curves). Thus, Ta was proved to be essential in preventing Cu from segregating out to the surface and Fe from being covered with Cu. Actually, Fe catalyst (2 nm) on TiN (15 nm) on a Cu foil without Ta interlayer could hardly grow CNTs (Fig. 3.7). It is also clear that the Ti peak became strong (Fig. 3.6(f)) because of the dewetting of the Fe layer to form Fe particles, which exposed the TiN layer (for all orange, black and red curves). When we changed the TiN layer thickness (Fig. 3.6(i−l)), the Ti peak weakened (Fig. 3.6(j)) and the Ta peak became more pronounced (Fig. 3.6(k)) for a thin TiN layer (5 nm, green curves) while the Fe and Ti peaks remained strong (Fig. 3.6(i,j)) and the Ta peak did not appear (Fig. 3.6(k)) for 30 nm-thick TiN layer (blue curves). This indicates that the presence of the TiN was essential for preventing Ta from segregating out to the top surface. Thus, the combination of TiN/Ta underlayers of proper thicknesses is effective in growing CNTs on Cu, as reported previously [55].

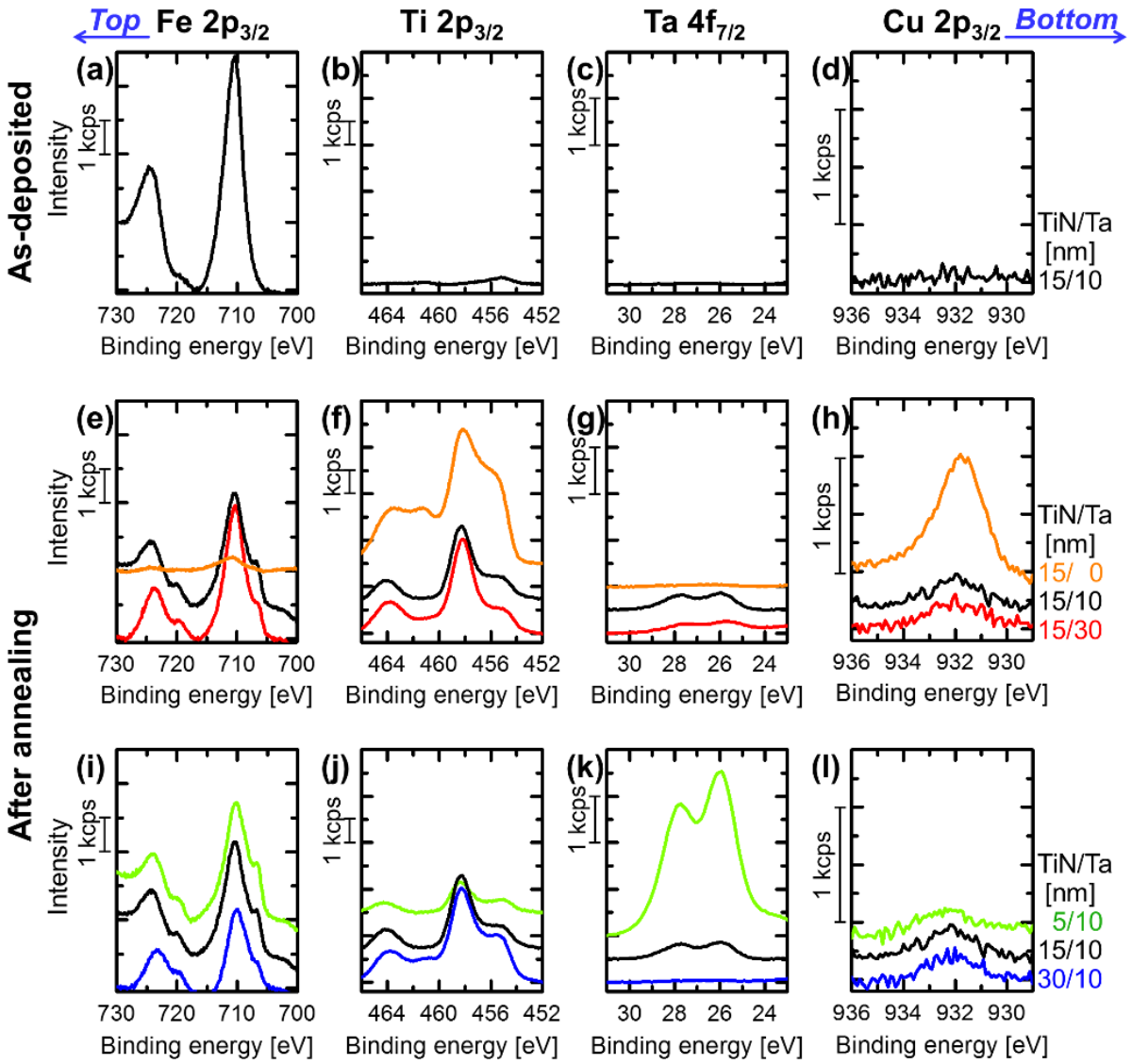

Fig. 3.6 XPS spectra for Fe (2.0 nm)/TiN (5–30 nm)/Ta (0–30 nm) layers on Cu foils as-deposited at R.T. (a–d) and after annealing at 700 ℃ (e–l).

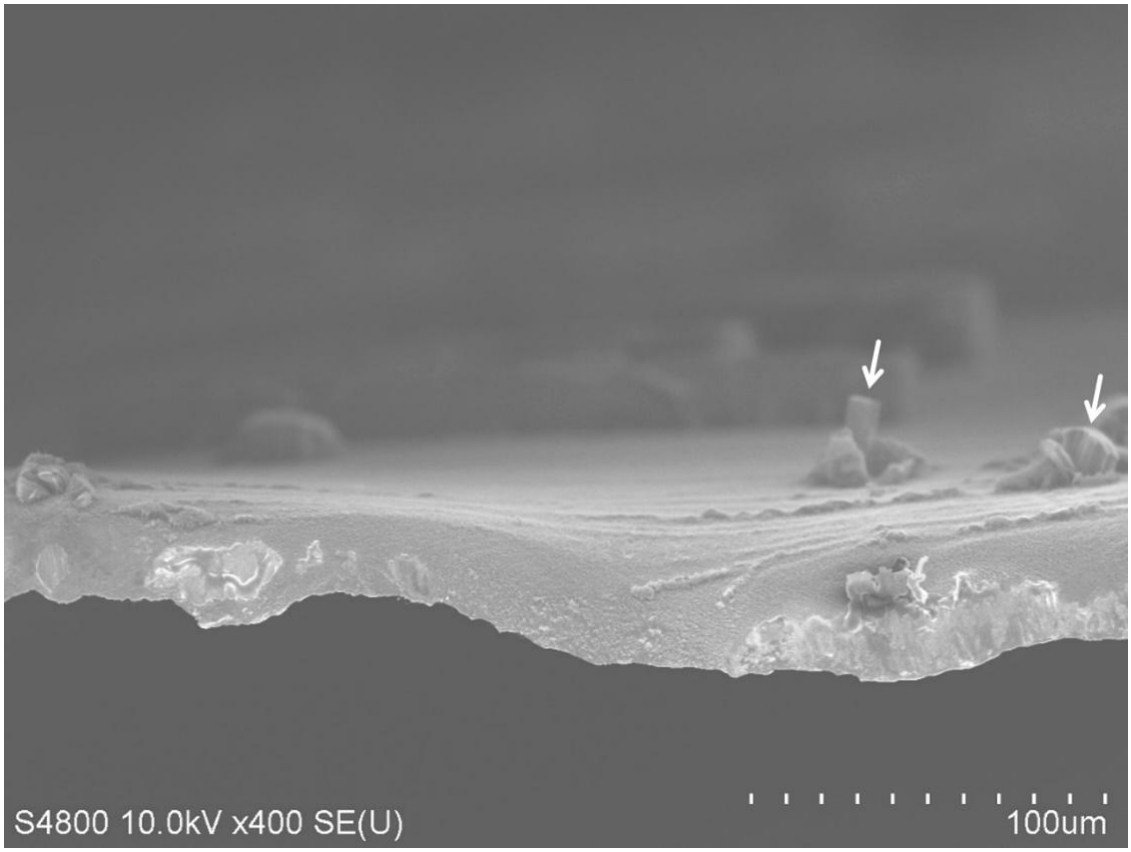

Fig. 3.7 A side-view SEM image of CNTs grown by Fe (2 nm) on TiN (15 nm) underlayer on a Cu foil from 27 Pa C_2H_2 at 700 °C for 30 min. The catalyst and underlayers were deposited at R.T. CNTs hardly grew; sub-μm-thick layer of entangled CNTs were observed over most region while CNT pillars of ~20 μm in height (marked with white arrows) were observed on some points.

From the results shown in Figs. 3.5 and 3.6, we set the bilayer of TiN (15 nm) on Ta (10 nm) as the standard underlayer for Fe catalyst and Cu foils. We then analyzed the crystal structure and electrical resistance of the underlayer. Fig. 3.8 shows the in-plane XRD spectra of Ta and TiN/Ta layers deposited on SiO_2/Si substrates. Ta and TiN layers were microcrystalline with in-plane grain size of ~2 and ~4 nm, respectively. The sheet resistances were measured by four-point-probe method and were 255 and 74.7 Ω/sq for the Ta and TiN/Ta layers, respectively. Because TiN and Ta layers were in a parallel configuration and the resistance normal to the film was negligible due to the small thickness, the sheet resistances of 255 and 106 Ω/sq and the resistivities of 255 and 158 μΩ cm were derived for the 10-nm-thick Ta and 15-nm-thick TiN,

respectively. These resistivity values were one-order of magnitude larger than their bulk properties of 12.3 and 21.7 μΩ cm due to their microcrystalline nature of the TiN/Ta underlayers prepared by sputter-deposition at ambient temperature and their small thickness. Their diffusion barrier performance may be improved further by controlling their crystal/amorphous structure.

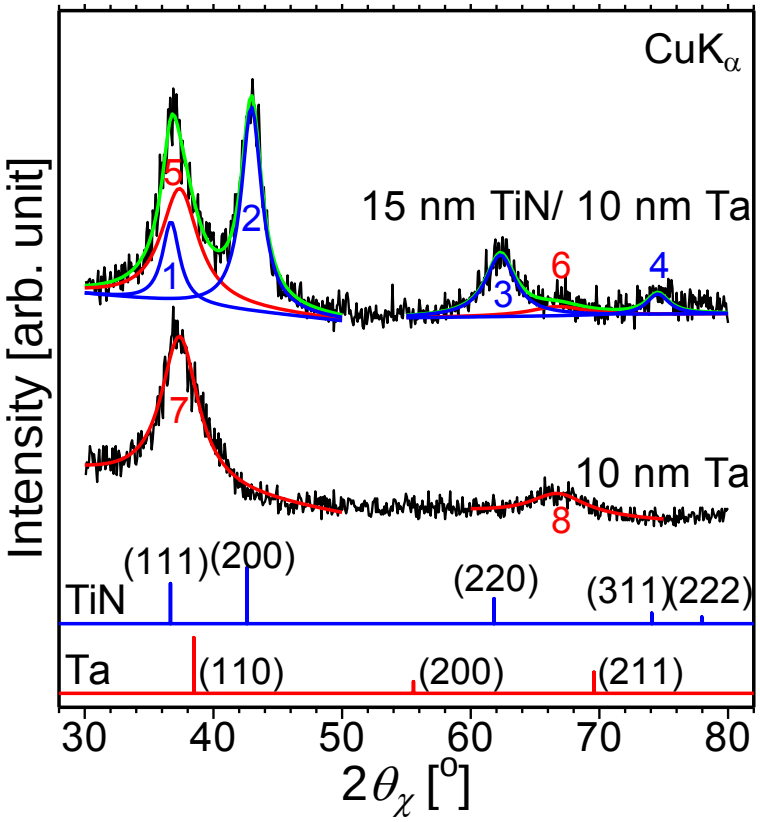

Standard data		Ta/SiO_2/Si			TiN/Ta/SiO_2/Si		
Peak	*d* [nm]	No.	*d* [nm]	*D* [nm]	No.	*d* [nm]	*D* [nm]
TiN (111)	0.2449				1	0.2447	4.88
TiN (200)	0.2121				2	0.2103	4.24
TiN (220)	0.1500				3	0.1489	3.15
TiN (311)	0.1279				4	0.1272	4.49
Ta (110)	0.2338	7	0.2404	2.26	5	0.2404	2.26
Ta (211)	0.1350	8	0.1400	1.71	6	0.1400	1.71

Fig. 3.8 In-plane XRD spectra of Ta and TiN/Ta layers formed on Si (100) wafers with 90-nm-thick thermal oxide layer. Ta (10 nm) and TiN (15 nm)/ Ta (10 nm) were deposited under the same condition as for the other experiments except for the substrate (i.e. SiO_2/Si in place of Cu). Because the peaks of Ta and TiN overlap with each other, in analyzing the TiN/Ta bilayer, the same values were used for the positions and widths of the Ta peaks as the Ta monolayer. The observed lattice constant, *d*, was somewhat larger than the standard data for Ta, showing the tensile stress or some incorporation of Ar or O atoms in the Ta layer while it was almost the same as the standard data for TiN. The in-plane grain size, D, was calculated from the band width at half maximum of the peak using Scherrer's equation with Scherrer constant of 0.85 (the value for Lorentz function).

3.3.3 Optimization of sputtering and CVD conditions for dense and tall CNT arrays

Next, we examined the conditions of Fe deposition on the TiN (15 nm)/Ta (10 nm)/Cu foil structures to control the Fe particle density. As we previously reported, application of substrate heating and substrate bias voltage is effective in preventing the catalyst particles becoming too densely deposited by promoting the surface diffusion of catalyst atoms, which results in the catalyst particles retaining high number density [34]. We therefore examined the structure of Fe particles deposited under different sputtering conditions and annealed at 700 °C under H_2/Ar using AFM (Fig. 3.9). For deposition at room temperature without bias voltage and high rate, large Fe particles with a low number density of 3.3×10^{11} cm^{-2} were observed after annealing (and thus prior to CVD) (Fig. 3.9(a)). Conversely, Fe particles deposited slowly on a heated substrate (400 °C) with bias voltage (−20 V) retained smaller size and higher density (8.0×10^{11} cm^{-2}) after annealing (Fig. 3.9(b)). The number density of Fe particles changed with the nominal Fe thickness and was highest (9.0×10^{11} cm^{-2}) for nominally 2.5 nm-thick Fe (Fig. 3.9(c)).

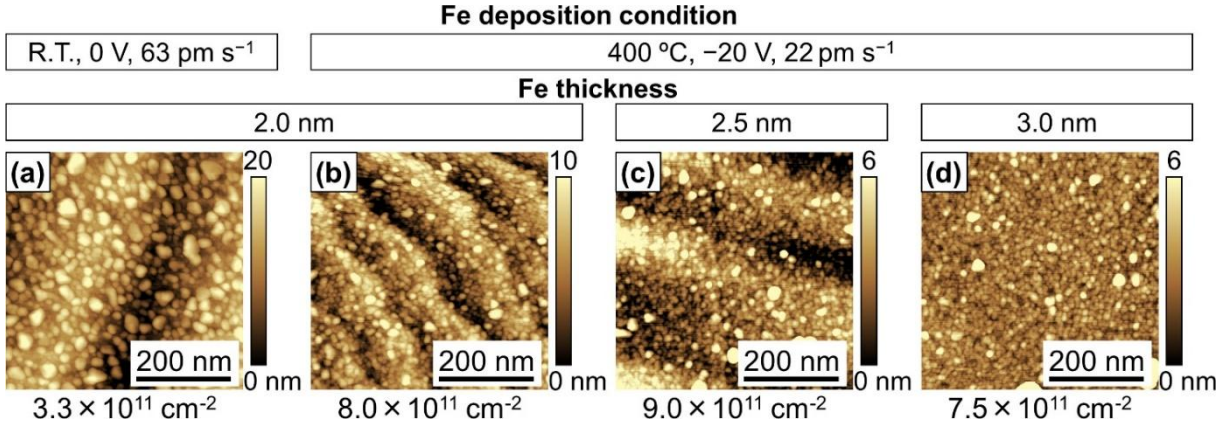

Fig. 3.9 AFM images of Fe particles on TiN (15 nm)/Ta (10 nm)/Cu foils deposited under different conditions and annealed at 4 kPa H_2 at 700 ℃ for 3 min.

We then grew CNT arrays using these Fe catalysts prepared under different conditions. Fig. 3.10 shows the side-view SEM images of the CNT arrays grown on Cu foils. Less dense Fe catalyst particles (Fig. 3.9(a)) yielded 70 μm-tall CNTs with a mass density of 0.21 g cm^{-3} (Fig. 3.10(a–c)), whereas the denser Fe catalyst particles (Fig. 3.10(c)) yielded shorter (45 μm) and denser (0.30 g cm^{-3}) CNT arrays (Fig. 3.10(f–h)). The areal mass of the resulting CNT arrays was similar; 1.48 mg cm^{-2} for Fig. 3.10(a–c) and 1.35 mg cm^{-2} for Fig. 3.10(f–h). SEM and scanning transmitting electron microscope (STEM) images were taken simultaneously to observe individual CNTs at a higher magnification (Fig. 3.10(d,e,i,j)). Some of the CNTs had catalyst particles on their tips while some did not (Fig. 3.10(e)), showing the coexistence of tip-growth and root-growth modes.

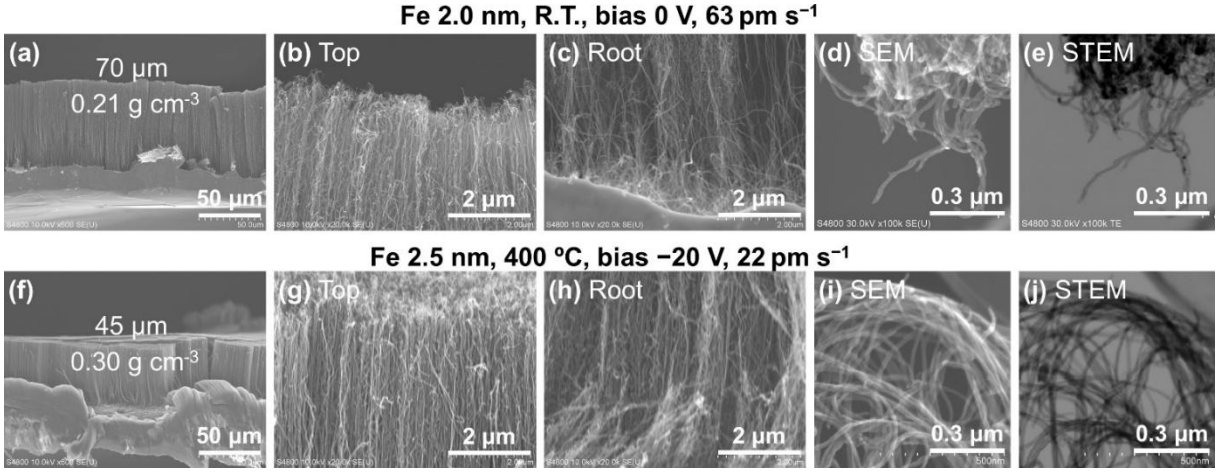

Fig. 3.10 Cross-sectional SEM images of the CNT arrays grown on Cu foils. Fe catalysts were deposited under two different conditions: (a–c) 2.0 nm in thickness, R.T., bias 0 V, and 63 pm s^{-1}, and (f–h) 2.5 nm in thickness, 400 °C, bias −20 V, and 22 pm s^{-1}, both with TiN (15 nm)/Ta (10 nm) underlayer on Cu foil (20 μm). CVD was carried out for 30 min using 27 Pa C_2H_2 at 700 °C.

Because the diameter and crystallinity of CNTs largely affect their thermal and electric conductivity, we characterized the CNTs grown on a Cu foil by HRTEM (Fig. 3.11). CNTs had a wide diameter distribution; many were 10−20 nm but some were ~5 and ~30 nm in diameter.

Some of the small-diameter CNTs had wavy walls (Fig. 3.11(b)) whereas some had smoother walls (Fig. 3.11(c)). Some of the large-diameter CNTs had smooth walls (Fig. 3.11(d)) whereas some had rougher walls (Fig. 3.11(e)). There was no clear corretation between the diameter and crystallinity (i.e. smoothness of the walls). Such differences in diameter and crystallinity might arise from the difference in the tip- and base-growth modes rather than the catalyst diameter, but further study is needed to clarify the key factor affecting the crystallinity of the CNTs.

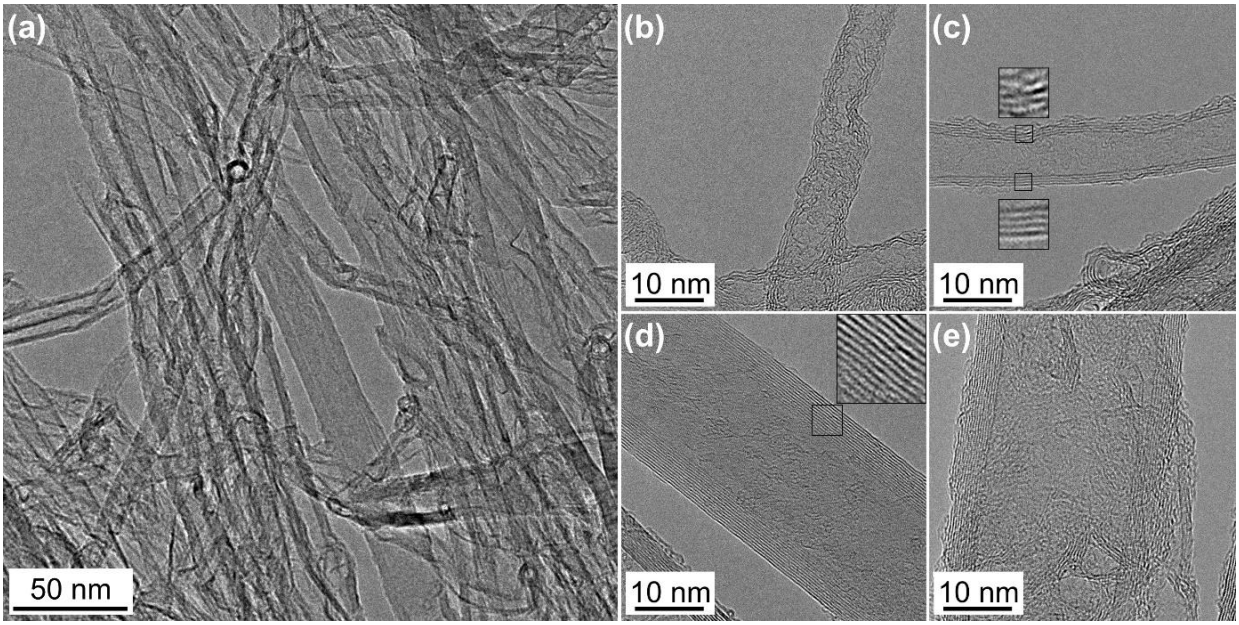

Fig. 3.11 TEM images of the CNTs grown on both faces of a Cu foil using the same catalyst and CVD conditions for Fig. 3.10 (f−j). (a) A low magnification TEM image and (b−e) HRTEM images. Inset in (c) and (d) are the magnified images (×3) showing the wall structures.

We then grew CNTs for different CVD durations, between 5 and 30 min. The CNTs grew taller linearly with time for all Fe catalysts (Fig. 3.12(a)), suggesting that 27 Pa C_2H_2 and 700 °C were appropriate conditions for keeping the Fe catalyst active and growing CNTs at a constant growth rate. However, the areal mass of CNTs became saturated at longer CVD time (Fig. 3.12(b)), resulting in decreasing mass density with increasing CNT height (Fig. 3.12(c)), similarly to our previous report [34]. The active catalyst particles should have retained a

constant activity, maintaining a constant growth rate in height, while the fraction of active catalyst particles should have decreased with the CVD time, resulting in decreasing growth rate in mass. This tradeoff between height and mass density is a crucial issue for obtaining taller and denser CNT arrays. CNT arrays with comparatively high density (0.21 g cm^{-3} at 61 μm) were obtained with 2 nm-thick Fe and 30 min CVD time. Among other CNT arrays with similar heights, the highest mass density was realized using the dense Fe catalyst particles (2.5 nm in thickness, Fig. 6(c)) deposited at 400 ℃, slow deposition rate (22 pm s^{-1}), and −20 V substrate bias.

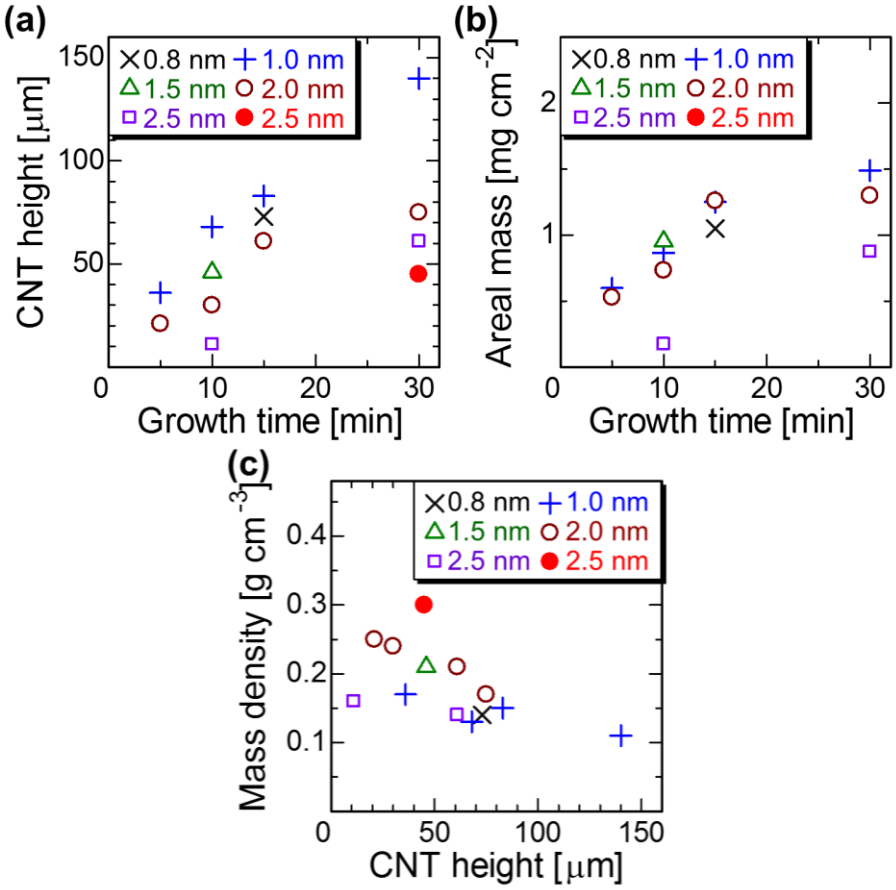

Fig. 3.12 (a) Growth time vs. CNT height, (b) growth time vs. areal density, and (c) CNT height vs. mass density of the CNT arrays grown at 26.7 Pa C_2H_2 and 700 ℃ using Fe catalysts with various thicknesses (0.8–2.5 nm) on TiN (15 nm)/Ta(10 nm)/Cu foils (20 μm). Fe was deposited at R.T., 0 V bias, and 63 pm s^{-1} except for the sample marked with a closed red circle (2.5 nm Fe catalyst, deposited at 400 ℃, bias −20 V, and 22 pm s^{-1}).

The results of the present work at different temperatures are shown in Fig. 3.1 with those of previous works [42, 49, 57, 58, 69-77]. For a wide range of CNT heights from several tens of nm to several mm, we can see a clear tradeoff between the height and mass density of CNT arrays. Catalyst particles can sit stable without coarsening but be easily deactivated by carbonization at low temperatures while they can be less easily carbonized but be easily coarsened at high temperatures [11]. Such tradeoff in catalyst stability between coarsening and carbonization together with the gradual deactivation of catalyst particles during CNT growth cause this tradeoff between the density and height of CNT arrays. Catalyst design for proper

catalyst underlayer (Figs. 3.4−3.6) and initial density of catalyst particles (Fig. 3.9) can enhance the mass density to some extent, as shown by the red arrow in Fig. 3.1 and the red closed circle in Fig. 3.12(c) (the same data shown in logarithmic and linear scales, respectively), but the growth of denser and taller CNT arrays is an ever-lasting challenge.

3.3.4 CNT array TIMs and their thermal resistances

Finally, the CNT arrays were grown on both faces of Cu foils to obtain CNT/Cu/CNT TIMs. Fig. 3.13(a) shows side-view SEM images of a typical TIM. The CNTs stood stable on the Cu foils even when handled with tweezers, indicating the good adhesion of the CNTs with the Fe/TiN/Ta/Cu structured substrate. Three factors were examined, the thickness of the Cu foil (10–80 μm), thickness of the CNT arrays (86–110 μm in total for both faces), and the mass density of the CNT arrays (0.05–0.26 g cm^{-3}). The thickness and mass density of the CNT arrays were controlled by changing the CVD time (10–30 min) and Fe catalyst thickness (0.8 nm and 2.0 nm), respectively (Fig. 3.13(b)). 20 μm-thick Cu foils with catalyst layers but without CNT arrays were used for comparison. The TIMs were set between Cu and Al blocks with a surface roughness of 20−30 μm (Fig. 3.2). The Cu foil without CNTs showed a high thermal resistance of 68 mm^2 K W^{-1}. For the low-density CNT arrays, the thermal resistance changed little and even increased to 86 mm^2 K W^{-1} for the CNT arrays of smallest mass density (0.05 g cm^{-3}). However, the thermal resistance decreased drastically from 86 to 24 mm^2 K W^{-1} with increasing CNT density from 0.05 to ~0.2 g cm^{-3} (Fig. 3.13(c)). No effect of the thickness of the CNT arrays (Fig. 3.13(d)) or Cu foils (Fig. 3.13(e)) was observed, showing that the Cu foils and CNT films had so small thermal resistance in bulk that the thermal resistance remained mostly at the interface, especially between the CNT arrays and metal blocks. It should

be noted that the CNT/Cu/CNT TIMs with CNT arrays of ~0.2 g cm^{-3} mass density exhibited a comparably low thermal resistance (24 mm^2 K W^{-1}) to that of a typical indium sheet TIM (100 μm in thickness, 18 mm^2 K W^{-1}), which means that the CNT arrays formed a good thermal interface with the Cu and Al blocks with surfaces as rough as 20−30 μm.

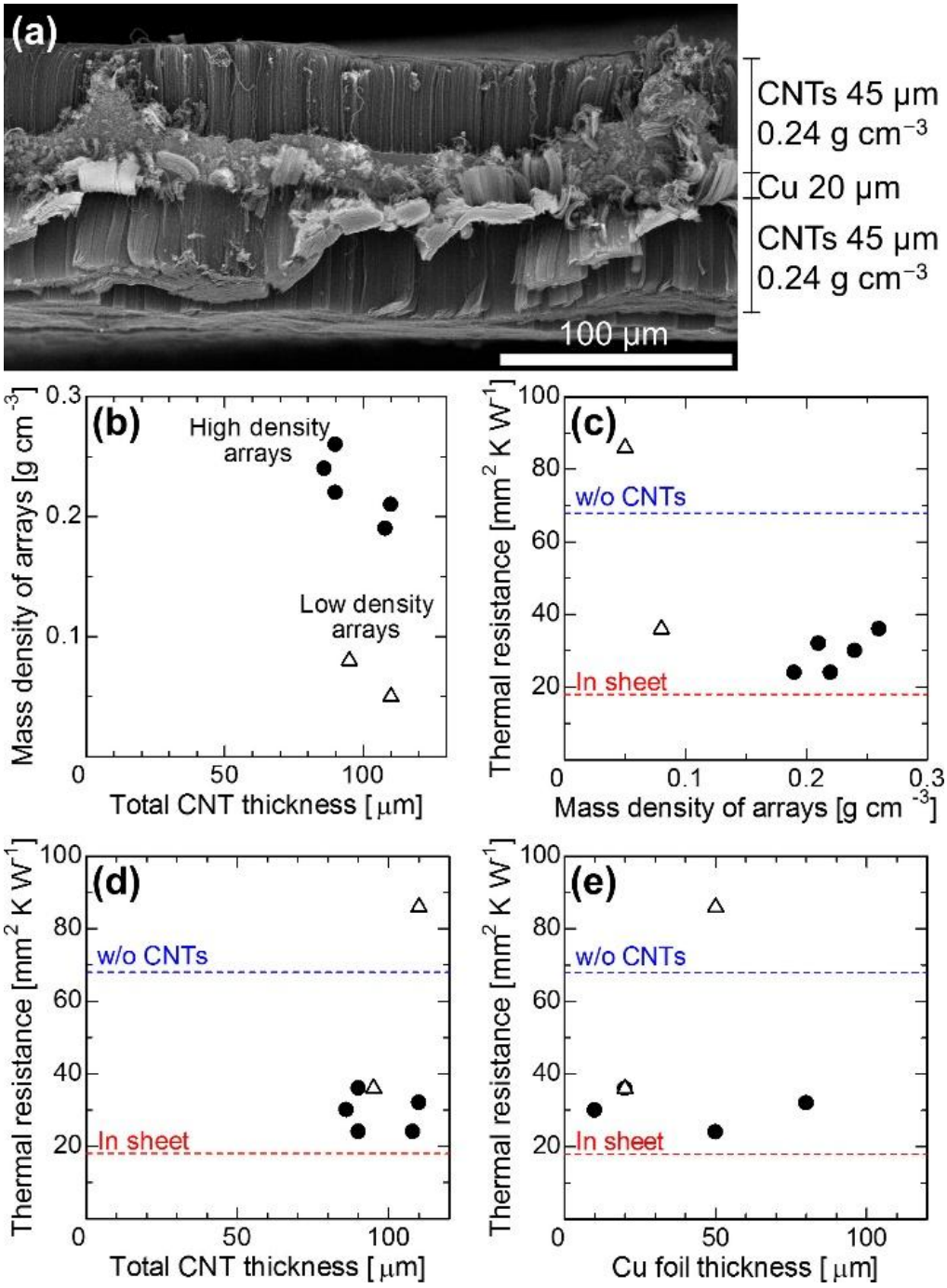

Fig. 3.13 (a) Side-view SEM images of typical CNT array TIMs. The CNT arrays were grown for 30 min using the same catalyst as Fig. 6(a). (b) Mass density of CNT arrays vs. total CNT thickness on both faces of Cu foils. (c) Thermal resistance vs. mass density of CNT arrays. (d) Thermal resistance vs. total CNT thickness. (e) Thermal resistance vs. Cu thickness. Closed circles: TIMs with high density CNT arrays. Open triangles: TIMs with low-density CNT arrays. Thermal resistance was measured under a pressure of 0.34 MPa. The thermal resistance values of TiN (15 nm)/Ta (10 nm) on Cu foils (20 μm) without CNT arrays and of a typical indium sheet TIM (100 μm in thickness) are also shown for comparison.

3.4 Conclusions

We realized the growth of vertically aligned CNT arrays of several tens of μm in height on both faces of Cu foils by optimizing the catalyst/underlayers and CVD conditions. It was confirmed that Ta and TiN layers are essential as diffusion barriers for Cu and Ta, respectively, at a CVD temperature of 700 ℃. The number density of Fe particles on the substrates was increased from 3.3×10^{11} cm^{-2} to 9.0×10^{11} cm^{-2} through control of the Fe catalyst deposition conditions. CNT arrays with a mass density of 0.30 g cm^{-3} and a height of 45 μm were grown at an optimized C_2H_2 pressure. However, we observed a tradeoff between the height and mass density of the CNT arrays, not only for the arrays grown under a fixed condition for increasing growth time but also for the arrays grown at higher temperatures. Growth of denser and taller CNT arrays is an ever-lasting challenge. Finally, CNT array/Cu foil/CNT array TIMs were fabricated, and their thermal resistances with Cu and Al blocks with 20−30 μm roughness were characterized. The thermal resistance of the TIMs decreased from 100 to 24 mm^2 K W^{-1} with increasing CNT array density from 0.05 g cm^{-3} to ~0.20 g cm^{-3}. The best CNT/Cu/CNT TIMs showed a thermal resistance comparable with that of a typical indium sheet TIM. Further control in CNT array density toward better thermal interface performance is now underway.

Chapter 4 - Conclusions and Perspectives

CNTs have been studied broadly by many researchers because they possess great electrical and thermal properties. Especially, vertically aligned CNT arrays, grown by chemical vapor deposition (CVD) on catalyst-supported substrates, are attractive for electric and thermal transport due to their anisotropic, uni-directional structure, however they usually contain CNTs at a few vol% with air at >90 vol%. To pull out the potential of CNTs, dense CNT arrays must be grown on device substrates, which changes with target applications.

The catalyst particles were formed densely through nucleation and growth by sputtering, which was stopped prior to percolation of the catalyst particles. Low temperature growth of dense CNT arrays at 400 °C was realized by lowering C_2H_2 feed to 0.13−1.3 Pa so as not to kill the catalyst. While growth of tens-μm-tall dense CNT arrays were realized by elevating the temperature to 700 °C and C_2H_2 feed to 27 Pa. Trade-off between the height and mass density

of CNT arrays was also confirmed. Fig. 3.1 shows the mass density of CNT arrays with different heights of CNTs, which were grown at different growth temperatures (400, 500 and 700 ℃). It clearly indicates the trade-off between CNT height and mass density, and shows how difficult to grow dense CNT arrays at high temperatures where catalyst particles can easily get aggregated/coarsened.

In this research, two application targets were addressed; via interconnects in LSI and TIMs.

In case of via interconnects, high-density CNT arrays have to be grown on conductive underlayers at limited growth temperatures as low as 400 ℃. Although high-density CNT arrays have been reported, the electrical resistance of resulting CNT arrays is still too high. The main reason is in the defects or by-products introduced to CNTs during their growth at very low growth temperatures. We realized growth of high-density (~1 g cm^{-3}) CNTs at 400 ℃ on conductive TiN underlayer, but CNTs contained by-products and defects. Therefore, not only increasing density, but also decreasing their defects and by-product are needed to realize CNT-via interconnects in the future.

In case of CNT application to TIMs, it is not needed to grow CNTs at low temperatures but to grow them tall enough to fill the gap between the heat source and heat sink with rough surfaces. Tall CNT arrays have been reported by many groups, however, many of such arrays have very low density (0.03−0.07 g cm^{-3}) with much air. Some groups reported low thermal resistance using CNT/Cu/CNT-TIMs but for smooth surfaces of sub-μm roughness. In this work, we realized tall (~50 μm) and dense (0.2−0.3 g cm^{-3}) enough CNT arrays on both faces of Cu foils, for which an information-communication technology company confirmed comparably low

thermal resistances (high heat-conducting performance) with a typical TIM of indium sheets for 20−30-μm rough device surfaces.

Engineered catalyst preparation and chemical vapor deposition processes for CNTs with structures and process conditions meeting the requirements from the application side will realize practical use of CNTs in society.

Acknowledgement

Firstly, I would like to gratefully acknowledge my advisor, Professor Suguru Noda. When I was in a slump, he always waited and gave me accurate advices. I thank him for his patience and understanding. For five years, not only knowledge about research, I learned him many things; a right attitude as a scientist, skills for writing paper from A to Z, way of scientific discussion, thinking logically... I have no doubt these things will be great properties in my future. Also I

would like to thank my committee members Prof . Yukio Yamaguchi, Prof. Tatsuya Okubo, Assoc. Prof. Akira Miyoshi, Assoc. Prof. Masao Katayama, Prof. Shigeo Maruyama for their time and valued feedback.

I would also like to thank to all the various collaborators. I appreciate Prof. Yuichi Ikuhara and Dr. Yeong-Gi So for plan-view HRTEM observation of CNT arrays. And I also thank Mr. Shinpei Enomoto in Waseda University for HRTEM observation of individual CNTs, and Mr. Takahiro Goto in Waseda University for XRD analysis. I am grateful to Mr. Hideo Nakajima at Shimadzu for the conductivity measurement by AFM, and Dr. Xiaosong Zhou and Dr. Mizuhisa Nihei at Huawei technologies for thermal conductivity measurements.

I also want to thank all Noda group members. Osawa-san always helped me maintain and support apparatuses. Thank to a lot of his assist, I could progress my research efficiently. I have also thoroughly enjoyed discussing and collaborating with Lee-san. Additional thanks go to Chen-san, Ricardo-san, and other lovely lab members for encouraging me when I was depressed.

I also thank Japan society including The University of Tokyo for supporting by funding from GMSI and Honors Scholarship. And Mizuho securities providing me great residence for four years, so I could focus on my research. Thank you very much.

Finally, to all my friends and my family, thank you for supporting me in everything.

References

[1] S. Iijima. Helical microtubules of graphitic carbon. *Nature 354(6348),* pp. 56-58. 1991.

[2] M. S. Dresselhaus, G. Dresselhaus, R. Saito and A. Jorio. Raman spectroscopy of carbon nanotubes. *Physics Reports 409(2),* pp. 47-99. 2005.

[3] A. Jorio, R. Saito, J. Hafner, C. Lieber, M. Hunter, T. McClure, G. Dresselhaus and M. Dresselhaus. Structural (n, m) determination of isolated single-wall carbon nanotubes by resonant raman scattering. *Physical Review Letters 86(6),* pp. 1118. 2001.

[4] A. Jorio, P. T. Araujo, S. K. Doorn, S. Maruyama, H. Chacham and M. A. Pimenta. The kataura plot over broad energy and diameter ranges. *Physica Status Solidi (b) 243(13),* pp. 3117-3121. 2006.

[5] A. Thess, R. Lee, P. Nikolaev, H. Dai, P. Petit, J. Robert, C. Xu, Y. H. Lee, S. G. Kim and A. G. Rinzler. Crystalline ropes of metallic carbon nanotubes. *Science 273(5274),* pp. 483-487. 1996.

[6] T. Ebbesen and P. Ajayan. Large-scale synthesis of carbon nanotubes. *Nature 358(6383),* pp. 220-222. 1992.

[7] R. Savoy, J. Vazquez and R. Beyers. Cobalt-catalysed growth of carbon nanotubes with single-atomic-layer walls. *Nature 363*pp. 17. 1993.

[8] Q. Zhang, J. Huang, M. Zhao, W. Qian and F. Wei. Carbon nanotube mass production: Principles and processes. *ChemSusChem 4(7),* pp. 864-889. 2011.

[9] W. Ren, F. Li, J. Chen, S. Bai and H. Cheng. Morphology, diameter distribution and raman scattering measurements of double-walled carbon nanotubes synthesized by catalytic decomposition of methane. *Chemical Physics Letters 359(3),* pp. 196-202. 2002.

[10] R. M. Sundaram, K. K. Koziol and A. H. Windle. Continuous direct spinning of fibers of single-walled carbon nanotubes with metallic chirality. *Advanced Materials 23(43),* pp. 5064-5068. 2011.

[11] K. Hasegawa and S. Noda. Moderating carbon supply and suppressing ostwald ripening of catalyst particles to produce 4.5-mm-tall single-walled carbon nanotube forests. *Carbon 49(13),* pp. 4497-4504. 2011.

[12] Z. Chen, D. Y. Kim, K. Hasegawa and S. Noda. Methane-assisted chemical vapor deposition yielding millimeter-tall single-wall carbon nanotubes of smaller diameter. *ACS Nano 7(8),* pp. 6719-6728. 2013.

[13] K. Hasegawa and S. Noda. Millimeter-tall single-walled carbon nanotubes rapidly grown with and without water. *ACS Nano 5(2),* pp. 975-984. 2011.

[14] K. Hata, D. N. Futaba, K. Mizuno, T. Namai, M. Yumura and S. Iijima. Water-assisted highly efficient synthesis of impurity-free single-walled carbon nanotubes. *Science 306(5700),* pp. 1362-1364. 2004.

[15] S. Noda, K. Hasegawa, H. Sugime, K. Kakehi, Z. Zhang, S. Maruyama and Y. Yamaguchi. Millimeter-thick single-walled carbon nanotube forests: Hidden role of catalyst support. *Japanese Journal of Applied Physics 46(5L),* pp. L399. 2007.

[16] H. Sugime and S. Noda. Cold-gas chemical vapor deposition to identify the key precursor for rapidly growing vertically-aligned single-wall and few-wall carbon nanotubes from pyrolyzed ethanol. *Carbon 50(8),* pp. 2953-2960. 2012.

[17] S. Maruyama, R. Kojima, Y. Miyauchi, S. Chiashi and M. Kohno. Low-temperature synthesis of high-purity single-walled carbon nanotubes from alcohol. *Chemical Physics Letters 360(3),* pp. 229-234. 2002.

[18] Y. C. Choi, Y. M. Shin, Y. H. Lee, B. S. Lee, G. Park, W. B. Choi, N. S. Lee and J. M. Kim. Controlling the diameter, growth rate, and density of vertically aligned carbon nanotubes synthesized by microwave plasma-enhanced chemical vapor deposition. *Appl. Phys. Lett. 76(17),* pp. 2367-2369. 2000.

[19] Z. F. Ren, Z. P. Huang, J. W. Xu, J. H. Wang, P. Bush, M. P. Siegal and P. N. Provencio. Synthesis of large arrays of well-aligned carbon nanotubes on glass. *Science 282(5391),* pp. 1105-1107. 1998.

[20] A. Moisala, A. G. Nasibulin and E. I. Kauppinen. The role of metal nanoparticles in the catalytic production of single-walled carbon nanotubes—a review. *Journal of Physics: Condensed Matter 15(42),* pp. S3011. 2003.

[21] A. G. Nasibulin, P. V. Pikhitsa, H. Jiang and E. I. Kauppinen. Correlation between catalyst particle and single-walled carbon nanotube diameters. *Carbon 43(11),* pp. 2251-2257. 2005.

[22] R. Baker, M. Barber, P. Harris, F. Feates and R. Waite. Nucleation and growth of carbon deposits from the nickel catalyzed decomposition of acetylene. *Journal of Catalysis 26(1),* pp. 51-62. 1972.

[23] S. Hofmann, R. Sharma, C. Ducati, G. Du, C. Mattevi, C. Cepek, M. Cantoro, S. Pisana, A. Parvez and F. Cervantes-Sodi. In situ observations of catalyst dynamics during surface-bound carbon nanotube nucleation. *Nano Letters 7(3),* pp. 602-608. 2007.

[24] S. Hofmann, R. Blume, C. T. Wirth, M. Cantoro, R. Sharma, C. Ducati, M. Hävecker, S. Zafeiratos, P. Schnoerch and A. Oestereich. State of transition metal catalysts during carbon nanotube growth. *Journal of Physical Chemistry C 113(5),* pp. 1648-1656. 2009.

[25] H. Cheng, F. Li, G. Su, H. Pan, L. He, X. Sun and M. Dresselhaus. Large-scale and low-cost synthesis of single-walled carbon nanotubes by the catalytic pyrolysis of hydrocarbons. *Applied Physics Letters 72(25),* pp. 3282-3284. 1998.

[26] J. J. Vilatela and A. H. Windle. Yarn-Like carbon nanotube fibers. *Adv Mater 22(44),* pp. 4959-4963. 2010.

[27] S. Noda, H. Sugime, K. Hasegawa, K. Kakehi and Y. Shiratori. A simple combinatorial method aiding research on single-walled carbon nanotube growth on substrates. *Japanese Journal of Applied Physics 49(2S),* pp. 02BA02. 2010.

[28] J. E. Trancik, S. C. Barton and J. Hone. Transparent and catalytic carbon nanotube films. *Nano Letters 8(4),* pp. 982-987. 2008.

[29] K. Sekiguchi, K. Furuichi, Y. Shiratori and S. Noda. One second growth of carbon nanotube arrays on a glass substrate by pulsed-current heating. *Carbon 50(6),* pp. 2110-2118. 2012.

[30] M. Nihei, M. Horibe, A. Kawabata and Y. Awano. Simultaneous formation of multiwall carbon nanotubes and their end-bonded ohmic contacts to ti electrodes for future ULSI interconnects. *Japanese Journal of Applied Physics 43(4S),* pp. 1856. 2004.

[31] B. A. Cola, X. Xu and T. S. Fisher. Increased real contact in thermal interfaces: A carbon nanotube/foil material. *Applied Physics Letters 90(9),* pp. 093513. 2007.

[32] W. Z. Li, S. S. Xie, L. X. Qian, B. H. Chang, B. S. Zou, W. Y. Zhou, R. A. Zhao and G. Wang. Large-scale synthesis of aligned carbon nanotubes. *Science 274(5293),* pp. 1701-1703. 1996.

[33] Z. Pan, S. Xie, B. Chang, C. Wang, L. Lu, W. Liu, W. Zhou, W. Li and L. Qian. Very long carbon nanotubes. *Nature 394(6694),* pp. 631-632. 1998.

[34] N. Na, D. Y. Kim, Y. So, Y. Ikuhara and S. Noda. Simple and engineered process yielding carbon nanotube arrays with 1.2× 1013cm− 2 wall density on conductive underlayer at 400° C. *Carbon 81*pp. 773-781. 2015.

[35] M. Bedewy, E. R. Meshot, M. J. Reinker and A. J. Hart. Population growth dynamics of carbon nanotubes. *Acs Nano 5(11),* pp. 8974-8989. 2011.

[36] P. Kim, L. Shi, A. Majumdar and P. L. McEuen. Thermal transport measurements of individual multiwalled nanotubes. *Physical Review Letters 87(21),* pp. 215502. 2001. . DOI: 10.1103/PhysRevLett.87.215502.

[37] T. Y. Choi, D. Poulikakos, J. Tharian and U. Sennhauser. Measurement of thermal conductivity of individual multiwalled carbon nanotubes by the 3-omega method. *Applied Physics Letters 87(1),* pp. 013108-013108-3. 2005.

[38] X. J. Hu, A. A. Padilla, J. Xu, T. S. Fisher and K. E. Goodson. 3-omega measurements of vertically oriented carbon nanotubes on silicon. *J. Heat Transfer 128(11),* pp. 1109-1113. 2006.

[39] Q. Zhang, G. Chen, S. Yoon, J. Ahn, S. Wang, Q. Zhou, Q. Wang and J. Li. Thermal conductivity of multiwalled carbon nanotubes. *Physical Review B 66(16),* pp. 165440. 2002.

[40] J. Hone, M. Llaguno, N. Nemes, A. Johnson, J. Fischer, D. Walters, M. Casavant, J. Schmidt and R. Smalley. Electrical and thermal transport properties of magnetically aligned single wall carbon nanotube films. *Applied Physics Letters 77(5),* pp. 666-668. 2000.

[41] Y. Murakami, S. Chiashi, Y. Miyauchi, M. Hu, M. Ogura, T. Okubo and S. Maruyama. Growth of vertically aligned single-walled carbon nanotube films on quartz substrates and their optical anisotropy. *Chemical Physics Letters 385(3),* pp. 298-303. 2004.

[42] G. Zhong, T. Iwasaki, K. Honda, Y. Furukawa, I. Ohdomari and H. Kawarada. Low temperature synthesis of extremely dense and vertically aligned single-walled carbon nanotubes. *Japanese Journal of Applied Physics 44(4R),* pp. 1558. 2005.

[43] Y. Awano, S. Sato, M. Nihei, T. Sakai, Y. Ohno and T. Mizutani. Carbon nanotubes for VLSI: Interconnect and transistor applications. *Proceedings of the IEEE 98(12),* pp. 2015-2031. 2010.

[44] J. Robertson, G. Zhong, C. S. Esconjauregui, B. C. Bayer, C. Zhang, M. Fouquet and S. Hofmann. Applications of carbon nanotubes grown by chemical vapor deposition. *Japanese Journal of Applied Physics 51(1S),* pp. 01AH01. 2012.

[45] Z. Yao, C. L. Kane and C. Dekker. High-field electrical transport in single-wall carbon nanotubes. *Physical Review Letters 84(13),* pp. 2941. 2000.

[46] P. L. McEuen, M. S. Fuhrer and H. Park. Single-walled carbon nanotube electronics. *IEEE Transactions on Nanotechnology 1(1),* pp. 78-85. 2002.

[47] N. Hamada, S. Sawada and A. Oshiyama. New one-dimensional conductors: Graphitic microtubules. *Physical Review Letters 68(10),* pp. 1579. 1992.

[48] Y. Miyata, K. Yanagi, Y. Maniwa and H. Kataura. Optical evaluation of the metal-to-semiconductor ratio of single-wall carbon nanotubes. *The Journal of Physical Chemistry C 112(34),* pp. 13187-13191. 2008.

[49] D. N. Futaba, K. Hata, T. Namai, T. Yamada, K. Mizuno, Y. Hayamizu, M. Yumura and S. Iijima. 84% catalyst activity of water-assisted growth of single walled carbon nanotube forest characterization by a statistical and macroscopic approach. *The Journal of Physical Chemistry B 110(15),* pp. 8035-8038. 2006.

[50] H. Li, W. Yin, K. Banerjee and J. Mao. Circuit modeling and performance analysis of multi-walled carbon nanotube interconnects. *Electron Devices, IEEE Transactions on 55(6),* pp. 1328-1337. 2008.

[51] H. Sugime and S. Noda. Millimeter-tall single-walled carbon nanotube forests grown from ethanol. *Carbon 48(8),* pp. 2203-2211. 2010.

[52] P. B. Amama, C. L. Pint, S. M. Kim, L. McJilton, K. G. Eyink, E. A. Stach, R. H. Hauge and B. Maruyama. Influence of alumina type on the evolution and activity of alumina-supported fe catalysts in single-walled carbon nanotube carpet growth. *ACS Nano 4(2),* pp. 895-904. 2010.

[53] S. Sato, A. Kawabata, D. Kondo, M. Nihei and Y. Awano. Carbon nanotube growth from titanium–cobalt bimetallic particles as a catalyst. *Chemical Physics Letters 402(1),* pp. 149-154. 2005.

[54] S. Sato, A. Kawabata, T. Nozue, D. Kondo, T. Murakami, T. Hyakushima, M. Nihei and Y. Awano. Fabrication of carbon nanotube via interconnects at low temperature and their robustness over a high-density current. *Sensors and Materials 21(7),* pp. 373-383. 2009.

[55] Y. Yamazaki, M. Katagiri, N. Sakuma, M. Suzuki, S. Sato, M. Nihei, M. Wada, N. Matsunaga, T. Sakai and Y. Awano. Synthesis of a closely packed carbon nanotube forest by a multi-step growth method using plasma-based chemical vapor deposition. *Applied Physics Express 3(5),* pp. 055002 1-055002 3. 2010.

[56] S. Esconjauregui, M. Fouquet, B. C. Bayer, C. Ducati, R. Smajda, S. Hofmann and J. Robertson. Growth of ultrahigh density vertically aligned carbon nanotube forests for interconnects. *ACS Nano 4(12)*, pp. 7431-7436. 2010.

[57] G. Zhong, J. H. Warner, M. Fouquet, A. W. Robertson, B. Chen and J. Robertson. Growth of ultrahigh density single-walled carbon nanotube forests by improved catalyst design. *ACS Nano 6(4)*, pp. 2893-2903. 2012.

[58] H. Sugime, S. Esconjauregui, J. Yang, L. D'Arsié, R. A. Oliver, S. Bhardwaj, C. Cepek and J. Robertson. Low temperature growth of ultra-high mass density carbon nanotube forests on conductive supports. *Applied Physics Letters 103(7)*, pp. 073116. 2013.

[59] H. Sugime, S. Noda, S. Maruyama and Y. Yamaguchi. Multiple ``optimum'' conditions for {C}o–{M}o catalyzed growth of vertically aligned single-walled carbon nanotube forests. *Carbon 47(1)*, pp. 234-241. 2009.

[60] K. Yamada, A. Kaneko, H. Kato and Y. Homma. Vertically-aligned carbon nanotube growth using closely packed iron oxide nanoparticles. *Materials Express 2(3)*, pp. 257-260. 2012.

[61] M. Hu, S. Noda, Y. Tsuji, T. Okubo, Y. Yamaguchi and H. Komiyama. Effect of interfacial interactions on the initial growth of cu on clean SiO 2 and 3-mercaptopropyltrimethoxysilane-modified SiO 2 substrates. *Journal of Vacuum Science & Technology A: Vacuum, Surfaces, and Films 20(3)*, pp. 589-596. 2002.

[62] M. Hu, S. Noda, T. Okubo, Y. Yamaguchi and H. Komiyama. Structural and morphological control of nanosized cu islands on SiO 2 using a ti underlayer. *Journal of Applied Physics 94(5)*, pp. 3492-3497. 2003.

[63] P. B. Amama, C. L. Pint, L. McJilton, S. M. Kim, E. A. Stach, P. T. Murray, R. H. Hauge and B. Maruyama. Role of water in super growth of single-walled carbon nanotube carpets. *Nano Letters 9(1)*, pp. 44-49. 2008.

[64] V. Zhitomirsky, I. Grimberg, L. Rapoprt, R. Hultman, J. Sundgren, J. Greene, D. Bergstrom and I. Petrov. High-flux low-energy (≅ 20 eV) N 2 ion irradiation during TiN deposition by reactive magnetron sputtering: Effects on microstructure and preferred orientation. *J. Appl. Phys. 78*pp. 5395-5403. 1995.

[65] D. N. Futaba, K. Hata, T. Yamada, T. Hiraoka, Y. Hayamizu, Y. Kakudate, O. Tanaike, H. Hatori, M. Yumura and S. Iijima. Shape-engineerable and highly densely packed single-walled carbon nanotubes and their application as super-capacitor electrodes. *Nature Materials 5(12)*, pp. 987-994. 2006.

[66] G. D. Nessim, M. Seita, K. P. O'Brien, A. J. Hart, R. K. Bonaparte, R. R. Mitchell and C. V. Thompson. Low temperature synthesis of vertically aligned carbon nanotubes with electrical

contact to metallic substrates enabled by thermal decomposition of the carbon feedstock. *Nano Letters 9(10),* pp. 3398-3405. 2009.

[67] B. Bayer, C. Zhang, R. Blume, F. Yan, M. Fouquet, C. Wirth, R. Weatherup, L. Lin, C. Baehtz and R. Oliver. In-situ study of growth of carbon nanotube forests on conductive CoSi2 support. *J. Appl. Phys. 109(11),* pp. 114314. 2011.

[68] M. Nihei, A. Kawabata and Y. Awano. Direct diameter-controlled growth of multiwall carbon nanotubes on nickel-silicide layer. *Japanese Journal of Applied Physics 42(6B),* pp. L721. 2003.

[69] R. D. Bennett, A. J. Hart and R. E. Cohen. Controlling the morphology of carbon nanotube films by varying the areal density of catalyst nanoclusters using Block-Copolymer micellar thin films. *Advanced Materials 18(17),* pp. 2274-2279. 2006.

[70] L. Ci, R. Vajtai and P. Ajayan. Vertically aligned large-diameter double-walled carbon nanotube arrays having ultralow density. *The Journal of Physical Chemistry C 111(26),* pp. 9077-9080. 2007.

[71] R. Xiang, Z. Yang, Q. Zhang, G. Luo, W. Qian, F. Wei, M. Kadowaki, E. Einarsson and S. Maruyama. Growth deceleration of vertically aligned carbon nanotube arrays: Catalyst deactivation or feedstock diffusion controlled? *The Journal of Physical Chemistry C 112(13),* pp. 4892-4896. 2008.

[72] B. Zhao, D. N. Futaba, S. Yasuda, M. Akoshima, T. Yamada and K. Hata. Exploring advantages of diverse carbon nanotube forests with tailored structures synthesized by supergrowth from engineered catalysts. *Acs Nano 3(1),* pp. 108-114. 2008.

[73] B. Zhao, Z. Song and J. Yang. Tunable field emission properties of carbon nanotube arrays by engineering fe catalysts. *Materials Letters 63(29),* pp. 2556-2559. 2009.

[74] M. Bedewy, E. R. Meshot, H. Guo, E. A. Verploegen, W. Lu and A. J. Hart. Collective mechanism for the evolution and self-termination of vertically aligned carbon nanotube growth. *The Journal of Physical Chemistry C 113(48),* pp. 20576-20582. 2009.

[75] M. B. Jakubinek, M. A. White, G. Li, C. Jayasinghe, W. Cho, M. J. Schulz and V. Shanov. Thermal and electrical conductivity of tall, vertically aligned carbon nanotube arrays. *Carbon 48(13),* pp. 3947-3952. 2010.

[76] S. Dörfler, A. Meier, S. Thieme, P. Németh, H. Althues and S. Kaskel. Wet-chemical catalyst deposition for scalable synthesis of vertical aligned carbon nanotubes on metal substrates. *Chemical Physics Letters 511(4),* pp. 288-293. 2011.

[77] A. Kawabata, T. Murakami, M. Nihei, K. Yamabe and N. Yokoyama. Evaluation of thermal resistance of carbon nanotube film fabricated using an improved slope control of temperature profile growth. *Japanese Journal of Applied Physics 54(4),* pp. 045101. 2015.

[78] P. B. Amama, B. A. Cola, T. D. Sands, X. Xu and T. S. Fisher. Dendrimer-assisted controlled growth of carbon nanotubes for enhanced thermal interface conductance. *Nanotechnology 18(38),* pp. 385303. 2007.

[79] X. Liu, Y. Zhang, A. M. Cassell and B. A. Cruden. Implications of catalyst control for carbon nanotube based thermal interface materials. *Journal of Applied Physics 104(8),* pp. 084310. 2008.

[80] K. Zhang, Y. Chai, M. Yuen, D. Xiao and P. Chan. Carbon nanotube thermal interface material for high-brightness light-emitting-diode cooling. *Nanotechnology 19(21),* pp. 215706. 2008.

[81] B. A. Cola, J. Xu, C. Cheng, X. Xu, T. S. Fisher and H. Hu. Photoacoustic characterization of carbon nanotube array thermal interfaces. *Journal of Applied Physics 101(5),* pp. 054313. 2007.

[82] W. Lin, R. Zhang, K. Moon and C. Wong. Synthesis of high-quality vertically aligned carbon nanotubes on bulk copper substrate for thermal management. *Advanced Packaging, IEEE Transactions on 33(2),* pp. 370-376. 2010.

[83] F. Lu and J. Ting. Very rapid growth of aligned carbon nanotubes on metallic substrates. *Acta Materialia 61(6),* pp. 2148-2153. 2013.

[84] H. Wang, J. Feng, X. Hu and K. M. Ng. Synthesis of aligned carbon nanotubes on double-sided metallic substrate by chemical vapor deposition. *J Phys Chem C 111(34),* pp. 12617-12624. 2007.